scientific reports

Check for updates

OPEN

Cell wall stress delays yeast cell separation by altering septin dynamics and chitinase localization via the cell wall integrity pathway

Raúl García[1,3], José Manuel Rodríguez-Peña[1,3], Alba Mangas-Losada[2], Sonia Díez-Muñiz[1], Yuliya Petryk[1], Carlos R. Vázquez de Aldana[2]✉ & Javier Arroyo[1]✉

The Cell Wall Integrity (CWI) MAPK pathway in *Saccharomyces cerevisiae* is crucial for coordinating adaptive responses to cell wall stress. We investigated the effects of zymolyase (ZY), a cell wall-perturbing agent, on cell morphology and cell separation. Our findings reveal that sublethal ZY treatment transiently delays mother-daughter cell separation, leading to multibudded cell clusters. This phenotype, which is accompanied by initiation of a new budding cycle before cell separation is complete, was observed with cell wall perturbations but not with osmotic, oxidative, or ER stress. Genetic and molecular analyses indicate that this cell separation defect depends on phosphorylation-dependent activation of Slt2, the MAP kinase of the CWI pathway. The phenotype is not fully mediated by the primary transcriptional regulator of the pathway, Rlm1, suggesting that Slt2-dependent outputs beyond canonical Rlm1 transcription contribute to the response. We also show that ZY treatment is associated with altered spatiotemporal localization and dynamics of septin rings, as well as changes in the intracellular trafficking of key septal proteins. Notably, delivery of the endochitinase Cts1 to the bud neck is delayed, and the residence time of the exocyst subunit Exo84 and the myosin Myo2 at the septum is reduced. Despite altered protein trafficking, the transcriptional program governed by the daughter-specific transcription factor Ace2 remains largely unaffected. Our data are consistent with a cell-separation delay resulting from a coordinated response involving the CWI pathway, which correlates with changes in septin dynamics and cytokinetic protein trafficking. These findings, which suggest a mechanism that transiently halts cell separation when cell wall integrity is compromised, highlight a link between cell wall homeostasis and the regulation of cell division in yeast.

Keywords Yeast, Cell wall stress and morphogenesis, Cell wall integrity pathway, Cell separation, Septin assembly, Septum degradation

Fungal cells are surrounded by a cell wall, an essential and highly dynamic structure that determines cell shape and protects against lysis caused by internal turgor pressure and environmental stress. This structure undergoes continuous remodeling to adapt to changing growth conditions[1,2]. The essential role of the cell wall in fungal survival, combined with the absence of its components in mammals, makes it an attractive target for antifungal therapies[3,4]. Despite its essential function, progress in understanding the biosynthesis of cell wall components, especially the remodeling and crosslinking machinery, has been relatively slow[5]. Therefore, elucidating the molecular mechanisms underlying cell wall assembly and remodeling represents a promising strategy for developing novel antifungal agents[3]. Significant insights into the molecular machinery and regulatory networks governing fungal cell wall maintenance and morphogenesis have been gained through studies in the model organism *Saccharomyces cerevisiae*. During morphogenetic events, the cell must remodel its wall to support growth and shape changes[6]. This process involves breaking existing crosslinks and incorporating newly synthesized polysaccharides into the cell wall matrix through elongation, branching, and crosslinking, activities driven by transglycosylase enzymes[7].

[1]Departamento de Microbiología y Parasitología, Facultad de Farmacia, Universidad Complutense de Madrid, Madrid 28040, Spain. [2]Instituto de Biología Funcional y Genómica (IBFG), Consejo Superior de Investigaciones Científicas-Universidad de Salamanca (CSIC-USAL), Salamanca, Spain. [3]Raúl García and José Manuel Rodríguez-Peña contributed equally to this work. ✉email: c.vazquez@csic.es; jarroyo@ucm.es

Exposure to cell wall-perturbing agents triggers stress responses that activate compensatory mechanisms. These include increased cell wall synthesis, changes in polymer crosslinking, and broad transcriptional reprogramming. This response results in the induction of genes involved in cell wall biogenesis and remodeling, energy metabolism, morphogenesis, signal transduction, and stress adaptation[1,8–11]. These adaptive responses are conserved across fungi[12,13] and are clinically relevant, since they complicate the development of effective antifungal therapies based on cell wall inhibitors. A better understanding of these adaptive mechanisms could facilitate the identification of new cell wall targets and the development of more effective antifungal drugs.

These responses are primarily coordinated in yeast via the Cell Wall Integrity (CWI) MAP kinase pathway[1,10,11]. This pathway is triggered by a group of putative mechanosensors on the cell surface (Wsc1-3, Mid2, and Mtl1)[14], which interact with the GDP/GTP exchange factor Rom2 to activate the small GTPase Rho1. In turn, Rho1 activates the protein kinase Pkc1, triggering a MAP kinase cascade that culminates in the activation of the MAPK Slt2/Mpk1[1,15]. Slt2 phosphorylates two key transcription factors: the MADS-box transcription factor Rlm1[16], and the Swi4/Swi6 (SBF) complex[17]. Rlm1 drives the expression of most genes activated under cell wall stress, including its own gene[11,18]. SBF regulates gene expression during the G1/S-phase transition[17] and also contributes to the regulation of a small subset of cell wall stress-responsive genes through a non-catalytic function of Slt2[10,19].

During cell cycle progression, the CWI pathway is activated in polarized growth phases, such as budding and cytokinesis, where it regulates cell wall biosynthesis and actin cytoskeletal organization. Errors in cell cycle processes or in progression under unfavorable conditions can have catastrophic consequences for the cell. Moreover, growing evidence indicates a reciprocal regulatory relationship between the cell cycle network and the CWI pathway. An excellent review detailing this relationship was recently published[20]. Briefly, the CWI pathway, via the Slt2 MAP kinase, regulates cell cycle progression at multiple levels. During the G1/S transition, Slt2 interacts with the SBF complex, influencing both the co-regulation of periodic cell wall gene transcription and the subcellular localization of Swi6[21,22]. In addition, expression of the *WHI7* gene, which encodes a G1 transcriptional repressor, is impaired in the absence of Slt2[23]. Slt2 has also been proposed to participate in the morphogenesis checkpoint, where bud formation is delayed under adverse environmental conditions[24]. Furthermore, in the context of the G1/S transition, Slt2 phosphorylates and stabilizes the cyclin-dependent kinase (CDK) inhibitor Sic1 during nutrient limitation[25]. Slt2 also helps delay S-phase entry and maintain genomic integrity in response to heat stress[26]. Lastly, during the G2/M transition, Slt2 is involved in regulating the G2-phase transcriptional program in response to cell wall stress, acting through the transcription factor Hcm1[27]. Cytokinesis splits a mother cell into two daughter cells. In budding yeast, this process occurs late in the cell cycle and proceeds rapidly, involving coordinated actomyosin ring contraction and septum formation, followed by septum degradation. Although the role of the CWI pathway in septum assembly is well established[28], a detailed understanding of how Slt2 controls late cell division events, especially cell separation, remains lacking.

In conclusion, the CWI pathway acts as a master brake that halts cell cycle progression when cells face unfavorable conditions. However, the full set of molecular components and mechanisms linking the CWI pathway to the regulation of cell proliferation in response to changes in cell-surface integrity and morphogenesis has not yet been fully understood.

The yeast cell division cycle starts with a single unbudded cell, which then forms a bud. As the bud grows to nearly the size of the mother cell, the nucleus divides, and ultimately, the two cells separate to become two new unbudded cells. The site of cytokinesis is established in late G1 at the narrow mother–bud neck, where a specialized structure known as the septum forms, consisting of a structure critical for cell separation. After mitosis is completed, a primary septum (PS), composed mainly of chitin and synthesized by the chitin synthase Chs2p, is deposited to separate the mother and daughter cells physically. Coordinated with PS formation, two secondary septa (SS), which are structurally similar to the lateral cell wall and primarily composed of β-glucans, are synthesized on either side of the PS. Notably, the septum is destroyed only minutes after formation. The PS and parts of the SS are degraded from the daughter cell side by hydrolytic enzymes, including an endochitinase and glucanases, ultimately leading to cell separation (reviewed in Lesage and Bussey[29]. The expression of these septum-degrading enzymes is regulated by a Hippo-like signaling cascade known as the Regulation of Ace2 and Morphogenesis (RAM) network. This pathway includes the Cbk1 kinase as a central component, which is specifically activated in daughter cells of *S. cerevisiae* (reviewed in Weiss[30] and Howell et al.[31]). The RAM pathway activates the transcription factor Ace2, which drives the expression of a daughter-specific expression program that includes genes necessary for septum degradation[32,33], such as *CTS1*, encoding the endochitinase Cts1. This secreted enzyme is essential for PS degradation and works together with the Eng1 endoglucanase to facilitate cell separation[34,35].

Recently, a checkpoint-like mechanism called ECO (Enforcement of Cytokinesis Order) has been identified. This pathway prevents Cts1 secretion in response to cytokinesis defects, functioning independently of Cbk1-mediated transcriptional control via the RAM pathway. ECO acts, at least in part, through Fir1-dependent inhibition of Cbk1 that could prevent Cts1 secretion when septation is disrupted[36]. In a closely related regulatory layer, TORC1 was recently shown to negatively regulate the NDR kinase Cbk1 and cell separation by altering Cbk1 phosphorylation and by controlling the Sec3/exocyst-SNARE axis that promotes membrane fusion of secretory vesicles transporting hydrolases to the division site[37]. In budding yeast, secretory vesicles are transported from the trans-Golgi network to the plasma membrane at the mother–bud neck along actin cables via the class V myosin Myo2. These vesicles are then tethered to the membrane by the exocyst, a conserved multimeric complex with eight subunits[38]. However, how cell wall stress signaling impinges on this exocytic control layer remains incompletely understood.

In the context of cytokinesis, a key structural element located at the bud neck, conserved mainly across eukaryotes, is the septin cytoskeleton. Septins are GTP-binding proteins that assemble into heteropolymers and are considered a component of the cytoskeleton[39]. These proteins are essential for many cellular processes,

including mitosis, exocytosis, cytokinesis, and cell morphogenesis, by acting as scaffolds and/or diffusion barriers, highlighting the complexity of their functional characterization (reviewed in Marquardt et al.[40]). In the budding yeast *S. cerevisiae*, seven septins have been identified, five of which (Cdc3, Cdc10, Cdc11, Cdc12, and Shs1) are expressed in mitotically active cells. Reflecting the intricate nature of septin function, these proteins are dynamically remodeled at the division site throughout the cell cycle. This reorganization is controlled by post-translational modifications (PTMs) and interactions with septin-associated proteins (SAPs)[40].

In this study, we examine the effect of acute cell wall stress on cell separation. Our data support the conclusion that zymolyase-induced cell wall stress causes a transient delay in mother–daughter separation, which depends on the activity of the MAPK Slt2. This phenotype is associated with altered septin dynamics and altered timing of Cts1 and the exocytic machinery at the division site. Thus, the present study contributes to a better understanding of how cells coordinate cell separation with cell wall integrity status.

Results and discussion

Cell wall stress induces a temporary delay in mother-daughter cell separation that depends on the CWI MAPK pathway

Previous studies employing high-dimensional quantitative morphological analysis of *S. cerevisiae* treated with cell wall-perturbing agents have demonstrated that different stress conditions elicit characteristic morphological alterations[41]. This approach has been successfully used to predict and identify the molecular targets of antifungal compounds such as poacic acid, which binds to β−1,3-glucan[42], and echinocandin B, a known β−1,3-glucan synthase inhibitor[41].

Building on these insights, we investigated whether exposure to zymolyase (ZY), a well-characterized agent that disrupts yeast cell wall integrity (consisting of an enzymatic cocktail with predominant β−1,3-glucanase activity), also triggers distinct morphological alterations. Wild-type cells were grown in liquid media with or without a sublethal concentration of ZY and monitored by optical microscopy at various time points up to 6 h. As shown in Fig. 1a, cells exposed to ZY displayed a clear cell separation defect, characterized by tri-cellular clusters consisting of two daughter cells attached to a single mother cell. This phenotype was absent in untreated controls, which typically showed mother cells with a single bud. Quantitative analysis of this phenotype, based on counting the frequency of multibudded cells over time, indicated that untreated cells rarely exhibited this feature, as expected. Conversely, ZY-treated cells exhibited the phenotype after 60 min, peaking at approximately 25% of the population between 180 and 210 min before gradually declining. These results suggest that the delay in cell separation is transient. Staining the cells with Calcofluor White (CFW), a chitin-binding fluorescent dye, confirmed that daughter cells in the multibudded clusters remained attached to the mother cell via chitin-rich septa at the bud neck, while nuclear segregation appeared normal, as assessed by DAPI staining (Fig. 1b).

To analyze the cell separation defect in a synchronized population, we arrested cells in G1 using α-factor, allowing us to monitor the dynamics of the separation phenotype upon release in the presence or absence of ZY. At 120 min post-release, corresponding to the completion of the first cell division, we observed an abrupt increase in cells initiating a new budding cycle without separating from the previous daughter cell. This phenotype peaked at nearly 60% of the population by 150 min and then declined, mirroring the pattern observed in asynchronous cultures (Fig. 1c). Similarly, when cells were arrested in S-phase as large-budded doublets with hydroxyurea and subsequently released into ZY-containing media, they completed division and entered a new round of cell division, again exhibiting the cell separation defect and subsequent rebudding (Fig. S1).

To assess whether our zymolyase treatment affects cell-cycle progression, BY4741 cells were synchronized in G1 with α-factor and then released into fresh medium in the presence or absence of zymolyase. Cell-cycle progression was monitored by quantifying the percentage of budded cells and by analyzing the levels of the cell-cycle regulators Sic1 and Clb3. Although a slight decrease in budded cells was observed at later time points in the zymolyase-treated culture (coincident with the appearance of multibudded cells), the overall budding profile was comparable between the two conditions (Fig. S2a). Moreover, the dynamics of both Sic1 and Clb3 were largely preserved after zymolyase treatment (Fig. S2b). Thus, zymolyase does not substantially interfere with the timing of budding, Sic1 degradation, or Clb3 accumulation in synchronized BY4741 cells. Together, these results indicate that zymolyase treatment does not cause a major delay or disruption in cell-cycle progression under these experimental conditions.

Collectively, our data indicate that ZY-treated cells complete division and initiate a new budding cycle before mother–daughter separation occurs, consistent with a delay in the final cell-separation step. Thus, ZY treatment, likely as part of an adaptive response to cell wall damage, temporarily delays cell separation in large-budded cells. Interestingly, a recent study reported that the Whi7 protein, previously characterized as a transcriptional repressor active during G1, also contributes to the formation of multibudded cells following prolonged (6-hour) exposure to CFW[43]. These authors showed that Whi7 becomes unstable under cell wall stress and that its degradation facilitates cell cycle re-entry, leading to a multibudded phenotype. This phenotype appears similar to that described in our work but differs significantly in the percentage of cells exhibiting it and in the timing of its appearance and recovery to baseline levels. ZY treatment affected fewer cells, and the phenotype appeared earlier and was more transient. Importantly, we observed that the *whi7*Δ mutant strain behaved similarly to the wild-type strain in both the frequency and timing of multibudded cell formation (Fig. S3), suggesting that, in contrast to the more persistent phenotype described for CFW, Whi7 is not required for the early, transient multibudding response to ZY under our conditions. Although we cannot rule out that differences between the two studies could partly stem from different yeast genetic backgrounds (BY4741 vs. W303), these differences might also arise because the dynamics of cell wall damage differ between CFW and ZY[11]. In fact, although cell wall damage caused by both ZY and CFW induces a primary response related to adaptation to cell wall integrity defects, regulated by the MAPK Slt2 and the transcription factor Rlm1, the cell wall transcriptional adaptive response to ZY requires the sequential activation of the Sho1 branch of the High Osmolarity Glycerol (HOG)

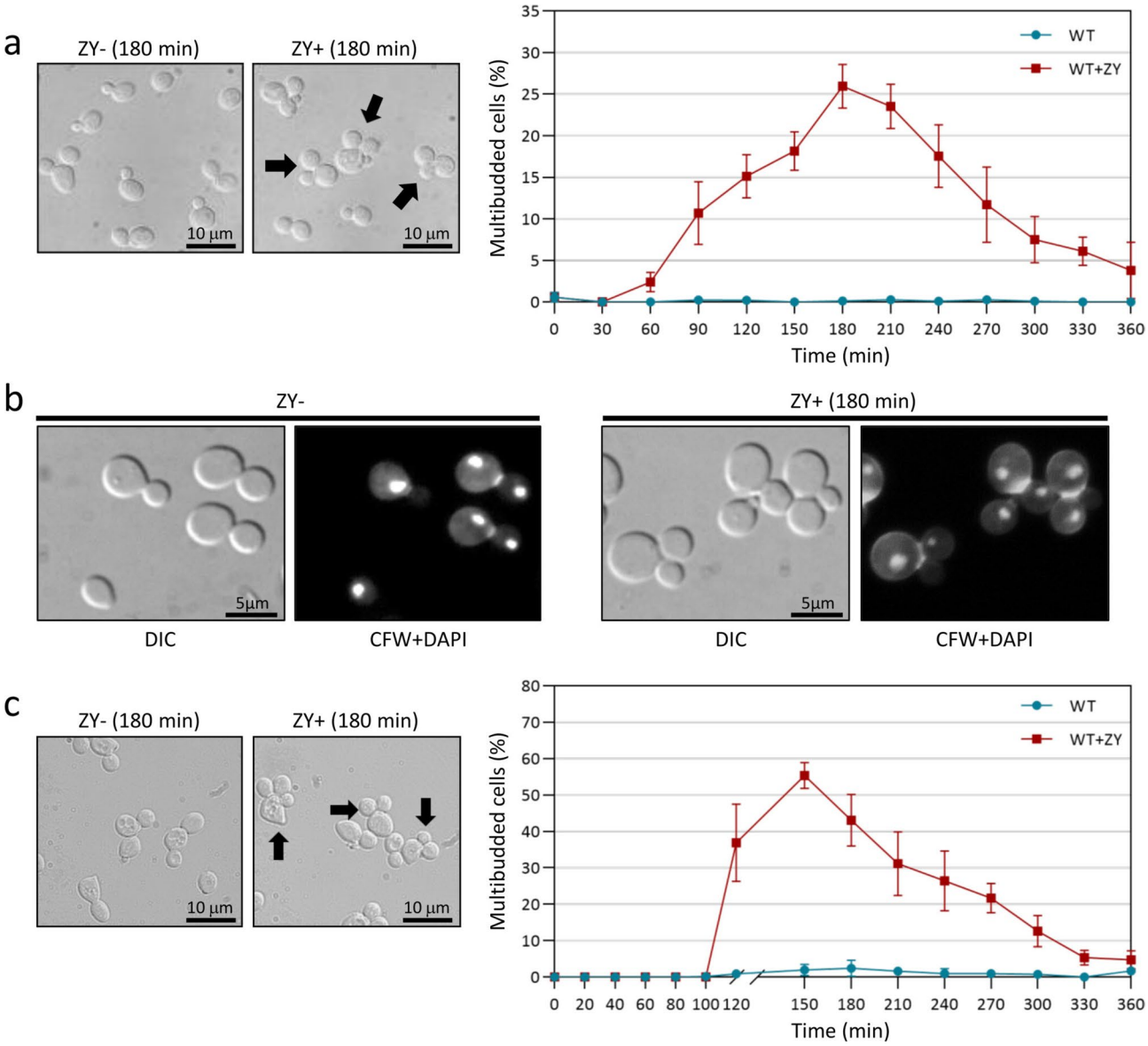


Fig. 1. Exposure to zymolyase promotes the formation of multibudded cells. **(a)** Cultures of the wild-type (WT) strain BY4741 grown exponentially were treated (ZY+) or not (ZY-) with 0.8 U/mL zymolyase (ZY) for 180 min and observed by differential interference contrast (DIC) microscopy (left panel). The proportion of multibudded cells was quantified over a time course from 0 to 360 min in the presence or absence of 0.8 U/mL ZY (right panel). **(b)** Fluorescence and DIC microscopy images of WT cells treated or untreated with ZY, stained with Calcofluor White (CFW) to visualize chitin deposition in the cell wall and septa, and with DAPI to visualize nuclear DNA. **(c)** Exponentially growing WT cultures were synchronized in G1 phase with α-factor and then released from cell-cycle arrest, either with or without ZY. Multibudded cells were counted over a 360 min time course (right panel). DIC images corresponding to the 180 min time point are shown (left panel). All data are shown as the mean ± standard deviation (SD) from three independent biological replicates. Black arrows indicate examples of multibudded cells. Scale bars = 10 µm **(a** and **c)** or 5 µm **(b)**.

pathway and the CWI[44]. Notably, the timing of multibudded cell formation in our study closely matches the activation kinetics of the CWI MAPK pathway, which orchestrates the primary adaptive response to cell wall stress. Specifically, a peak in phosphorylated (active) Slt2, the MAP kinase of this signaling cascade, occurs within 2–3 h after ZY exposure[44].

To obtain a more detailed view of the neck region separating mother and daughter cells in α-factor-synchronized cells exhibiting the separation phenotype after 3 h of ZY exposure, transmission electron microscopy was used (Fig. 2). The images revealed minor alterations in the overall septum structure. After the PS is completed, SS are formed on both the mother and daughter sides[45]. Their composition is probably similar to that of lateral cell walls[7]. In ZY-treated cells, the chitin-based PS synthesized by Chs2, which appears as a less electron-dense white band, has a similar appearance/structure to that of untreated cells, whereas the SS does not.

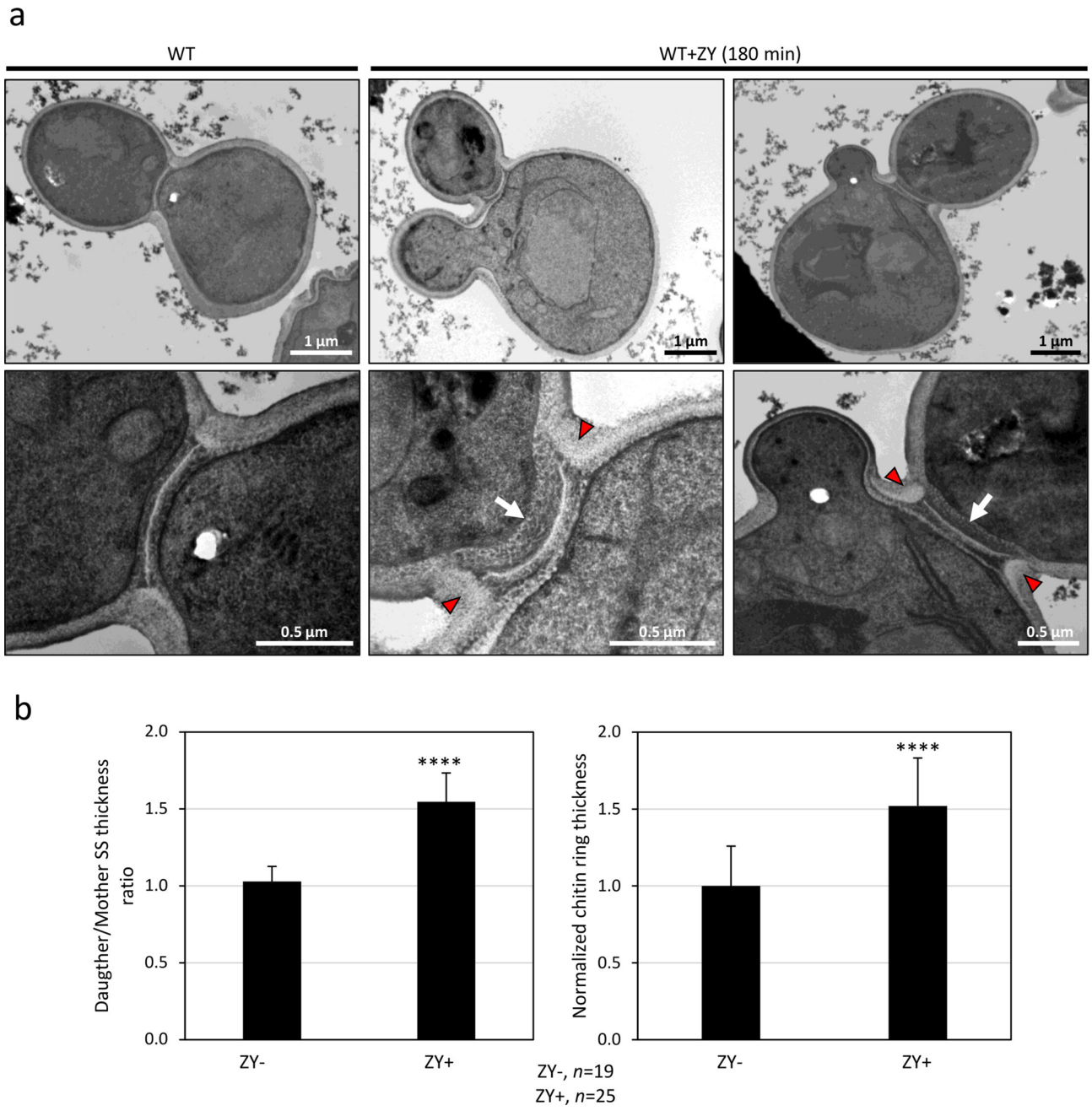


Fig. 2. Zymolyase causes asymmetric thickening of the secondary septum and thickening of the chitin ring. **(a)** Exponentially growing cultures were synchronized in G1 phase with α-factor and then released from cell-cycle arrest in the presence or absence of ZY for 180 min. Cells were subsequently prepared for transmission electron microscopy. The micrographs in the second row provide enlarged views of the septal regions corresponding to the cells shown above. Red arrowheads mark septal regions displaying chitin ring thickening. White arrows indicate areas of secondary septum (SS) thickening on the daughter-cell side. Representative cells for each condition are shown. Scale bars: 1 µm (top) and 0.5 µm (bottom). **(b)** Quantitative analysis of septal dimensions is shown. The left graph represents the ratio of daughter to mother SS thickness. The right graph shows the normalized chitin ring thickness of ZY-treated cells relative to the ZY- control (set to 1). Data are presented as mean ± SD ($n = 19$ for ZY-; $n = 25$ for ZY+). Statistical significance was determined using a two-tailed unpaired Student's t-test comparing ZY+ with no treatment (****$P \leq 0.0001$).

The normally symmetrical distribution of the SS on both sides observed in untreated cells appeared altered in a subset of ZY-treated cells exhibiting the phenotype (~ 83,3%, $n = 25$). Thus, ZY caused a thickening of the SS in the older daughter cells of the triplets, which was 50% wider than on the mother side (Fig. 2). Additionally, ZY-treated cells exhibited a thickening (1.5 fold) of the chitin ring at the bud neck (Fig. 2), consistent with increased chitin deposition associated with the compensatory response to cell wall stress[46].

To quantify the delay in the separation of the first daughter cell in ZY-treated cells, at the single-cell level, we performed time-lapse microscopy experiments using a microfluidic platform (see Methods for details). These experiments were conducted with a strain carrying an integrated mRuby2-Tub1 fusion, which labels the mitotic spindle, together with an Mlc2-mApple fusion, used as a marker of the actomyosin contractile ring, thereby allowing simultaneous monitoring of contractile ring dynamics and spindle behavior. By using spindle breakage or disassembly as a temporal reference point (time "0") for each cell, we measured the time required for cell separation in both ZY-treated and untreated conditions. As shown in Fig. 3, the average separation time in untreated cells was approximately 15 min, whereas in ZY-treated cells exhibiting the phenotype, separation was significantly delayed, averaging around 105 min.

Next, we evaluated whether the cell separation defect observed following ZY treatment was specific to this compound or also occurred under other stress conditions. To do this, wild-type cells were incubated for 3 h in the presence of various stressors, including CFW (a chitin-binding dye), KCl (osmotic stress), hydrogen peroxide (oxidative stress), and tunicamycin, a glycosylation inhibitor that induces endoplasmic reticulum (ER) stress[47]. As shown in Fig. 4a, under the conditions tested, multibudded cells were observed only with treatments that perturbed the cell wall, namely ZY and CFW, but not with osmotic, oxidative, or ER stress treatments. Thus, our data support an association between this phenotype and the tested cell wall perturbations, without excluding the possibility that other stresses or conditions not examined here could also influence cell separation. Notably, thermally inactivated ZY[48] failed to induce the cell-separation phenotype, indicating that ZY enzymatic activity is necessary for triggering this morphological defect. Additionally, adding sorbitol to the growth medium restored normal cell separation in ZY-treated cells, supporting the conclusion that this phenotype stems from cell wall stress (Fig. 4a). This aligns with the well-established idea that osmotic stabilization (e.g., sorbitol addition) can alleviate defects caused by compromised cell wall integrity[8].

Once the association between cell wall damage and the cell separation phenotype was established, we moved to investigate the role of the CWI MAPK pathway in this process. To this end, we assessed the effect of ZY treatment in a strain lacking the MAPK of this pathway, Slt2; in cells expressing a kinase-dead (KD) version of Slt2, which cannot phosphorylate substrates; and in cells expressing the TA/YF version, which cannot be phosphorylated (i.e., activated) by the upstream MAPKKs of the pathway, Mkk1/2. As shown in Fig. 4b, all cases showed a drastic reduction in the percentage of clusters with three or more connected cells. When the *SLT2* deletion strain was transformed with a plasmid carrying the wild-type version of *SLT2*, the separation phenotype was restored to levels similar to those seen in the wild-type strain. These results demonstrate that both Slt2 activation and kinase activity are required for the development of the cell separation delay phenotype. Consistent with these observations, a yeast strain deleted for *SHO1*, a component of the activation cascade of the HOG MAPK pathway involved in the cellular response to high osmolarity and necessary for ZY-mediated Slt2 activation[44], showed almost complete absence of multibudded cells following ZY treatment. However, deletion of *RLM1*, the primary transcription factor regulated by the CWI pathway via Slt2, resulted in only a partial reduction (~ 50% compared to the WT strain) in the cell clustering phenotype (Fig. 4b). This supports the idea that the morphological phenotype is not fully mediated by Rlm1 and is not solely dependent on the transcriptional activation of canonical Rlm1 targets. Instead, it might reflect Slt2-dependent signaling outputs that extend beyond Rlm1-dependent transcription. Nevertheless, it cannot be ruled out that the partial effect observed in the absence of Rlm1 may, at least in part, be a consequence of its influence on Slt2 levels by disrupting the positive feedback loop through which Rlm1 enhances *SLT2* expression in ZY-stressed cells, as previously reported[18].

A similar, but more severe and lasting phenotype, characterized by the accumulation of cells with multiple successive buds, has recently been described in a mutant lacking the protein phosphatase Ptc1, grown at high temperature[49]. Our findings, in agreement with those of González-Rubio et al.[49], support the idea that hyperactivation of Slt2 in cells exposed to cell wall–damaging agents leads to a temporary delay in cell separation, specifically affecting daughter cells, potentially serving as an adaptive response to challenging environmental conditions. In our case (WT cells exposed to cell wall stress mediated by zymolyase), the phenotype is less severe, with a transitory delay in cell separation. However, in *ptc1*Δ cells, hyperactivation of the MAPK Slt2, caused by heat-mediated stress and the absence of the phosphatase that negatively regulates it (via dephosphorylation), results in multiple phenotypic traits, including a failure to undergo cell separation, perturbed mitochondrial inheritance, increased autophagy, TORC1-Sch9 inhibition, and daughter-specific G1 cell cycle arrest[49].

As in our case, these authors reported that cell separation defects observed in *ptc1*Δ cells subjected to heat stress are only partially attributable to the Rlm1-mediated response and suggested that other Slt2 substrates, distinct from Rlm1 and SBF (Swi4/Swi6), contribute to the multibudding phenotype.

Zymolyase treatment alters septin dynamics in unseparated mother–daughter cells

One of the most crucial structures at the bud neck (the constriction between mother and daughter cells) is the septin ring. The septin ring and the chitin ring have redundant functions in preventing cell wall growth at the mother-bud neck, where cytokinesis, septation, and cell division occur[7]. These highly conserved GTP-binding proteins assemble into various filament-containing structures, transitioning from a nascent ring at the presumptive bud site, to an hourglass shape at the bud neck, and finally splitting into a double ring flanking the cytokinetic machinery (revised in Tamborrini and Piatti[50] and Marquardt et al.[40]). Although current models propose that septins function as a cellular scaffold and/or diffusion barrier, the mechanisms controlling septin assembly and remodeling throughout the yeast cell cycle are still not fully understood.

To investigate a potential link between septin organization at the bud neck and the cell-separation phenotype induced by ZY treatment, we performed time-lapse confocal fluorescence microscopy to monitor the in vivo dynamics of septins in yeast cells displaying this phenotype. Images were acquired every 4 min using a strain expressing a genomically integrated version of the septin Cdc3 fused to the fluorescent protein mCherry. As

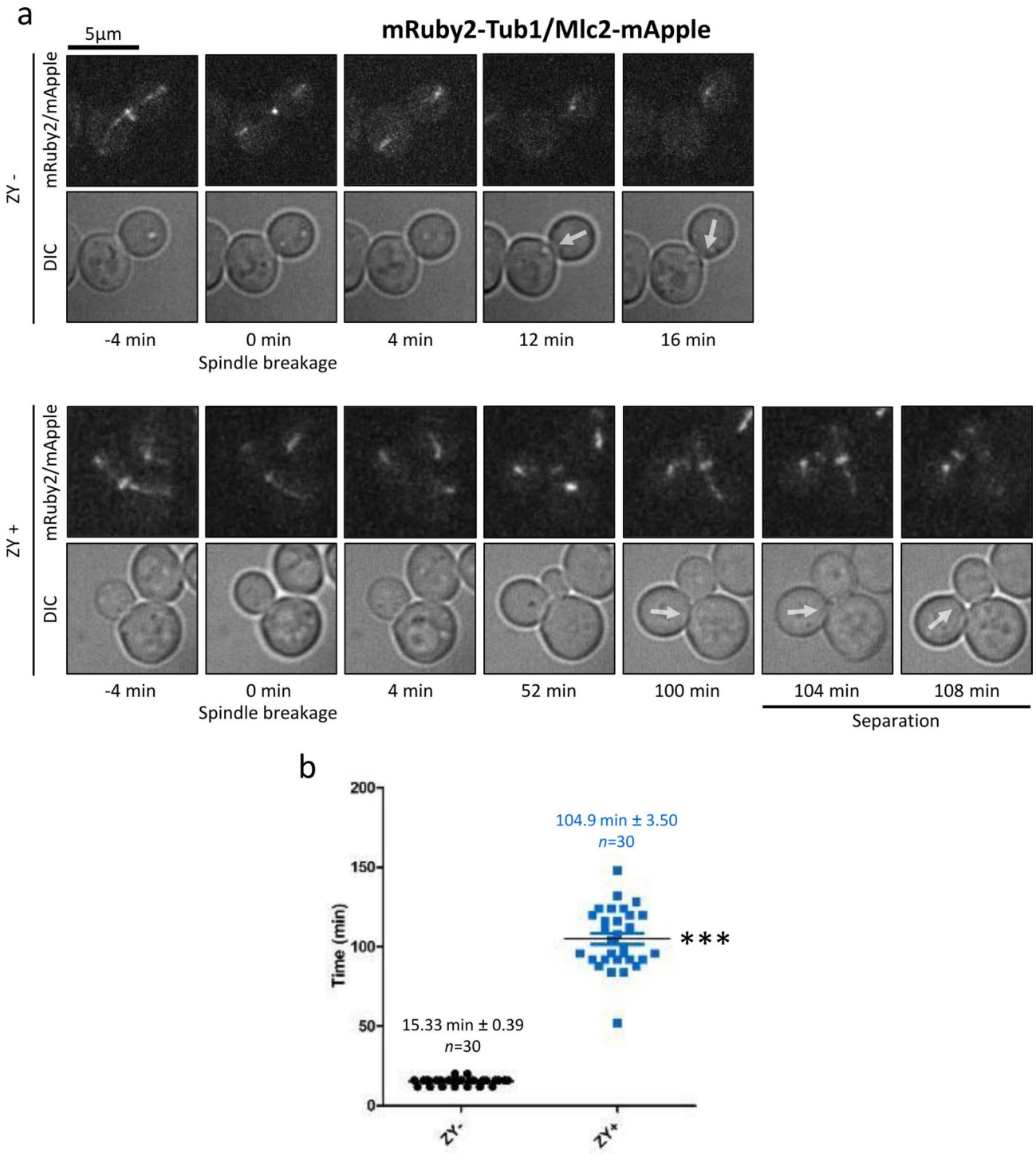
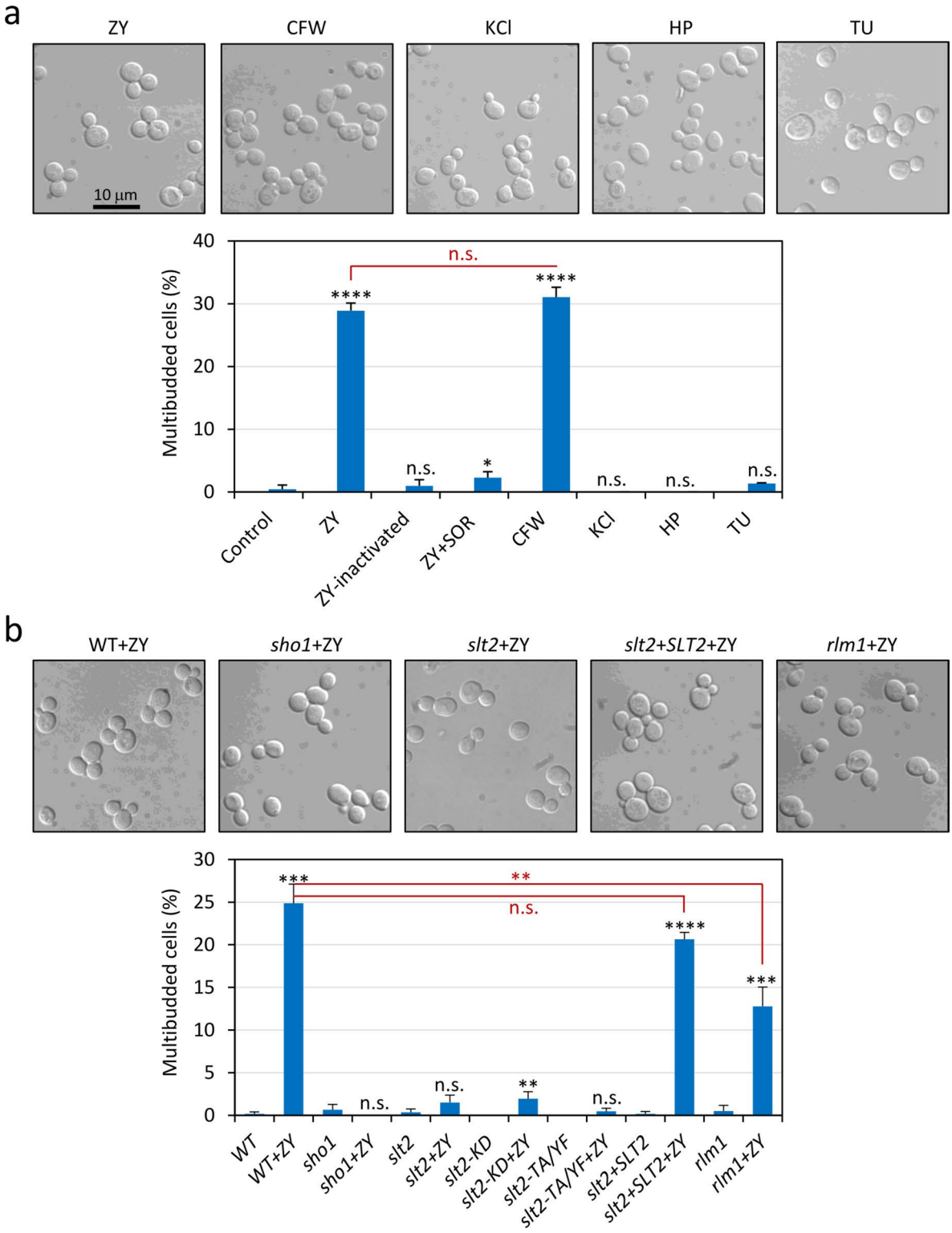


Fig. 3. Zymolyase induces a delay in cell separation. **(a)** Time-lapse images (DIC and confocal fluorescence microscopy) of individual cells expressing the mRuby2-Tub1/Mlc2-mApple fusion proteins, which mark mitotic spindle disassembly, were acquired using the ONIX2 microfluidic platform (see Methods for details). All single-cell data were time-synchronized at the moment of mitotic spindle disassembly, marked as time zero, as described previously[60]. Cell montages were assembled from selected frames taken at 4-minute intervals during the time-lapse series. Arrows indicate cell separation events, inferred from morphological changes in the older daughter cell. Representative time-lapse microscopy experiments are included. Scale bar = 5 µm. **(b)** Quantitative data from a larger number of cells, comparing the timing of cell separation with and without ZY, are shown in the scatter plots. Each dot represents an individual cell ($n = 30$ for ZY- and ZY+), with horizontal bars and numerical values indicating the mean ± Standard Error of the Mean (SEM). Statistical significance was tested using a two-tailed, unpaired, Student's *t*-test, comparing ZY+ with no treatment (***$P \leq 0.001$).



shown in Fig. 5, the timing and spatial distribution of Cdc3 in cells grown without ZY matched the expected pattern. At the end of cell division, the septin ring on the daughter-cell side disassembles and quickly reassembles at the new presumptive budding site[51]. Notably, in cells treated with ZY and displaying the separation phenotype, the septin ring on the daughter side of the neck failed to disassemble, whereas the mother-side septin collar disassembled just before a new septin ring formed at the next presumptive bud site (Fig. 5). This persistent mislocalization phenotype was observed in 100% of the cells analyzed ($n = 100$). Similarly, in multibudded cells of *ptc1*Δ cells growing at 38 °C, the two septin rings also exhibited asymmetrical disassembly[49].

Septins are considered part of the cytoskeleton that perform multiple vital roles in the cell, including during cytokinesis. The septin ring plays an essential role in this process, mainly serving as a scaffold for participating proteins, like Chs3, which ensures chitin ring formation[52,53], and Crh2, one of the enzymes responsible for the covalent linkage between glucan and chitin, at the neck[54]. It also acts as a physical barrier to prevent diffusion of

◀**Fig. 4**. The multibudded phenotype correlates with cell wall stress and relies on the activity of the CWI pathway. **(a)** The histogram shows the percentage of multibudded cells in the wild-type strain after 3 h of exposure to different cellular stressors. Control: untreated cells; ZY: 0.8 U/mL zymolyase; ZY-inactivated: 0.8 U/mL heat-inactivated zymolyase (100 °C, 15 min); ZY + SOR: 0.8 U/mL zymolyase supplemented with 1 M sorbitol; CFW: 10 µg/mL Calcofluor White; KCl: 550 mM potassium chloride; HP: 3 mM hydrogen peroxide; TU: 1 µg/mL tunicamycin. Representative DIC images are shown above the histogram. **(b)** The histogram shows the percentage of multibudded cells in the wild-type (WT) strain and in some mutant strains lacking components of the Cell Wall Integrity (CWI) pathway after 3 h of growth in the presence or absence of 0.8 U/mL ZY. The effect of different Slt2 alleles on the multibudded phenotype was examined using an *slt2*Δ strain transformed with plasmids expressing different Slt2 variants: a kinase-dead mutant (KD), a non-phosphorylatable mutant (TA/YF), the wild-type *SLT2*, or an empty vector. Representative DIC images are shown above the histogram. For **(a)** and **(b)**, data represent the mean ± SD from at least two independent experiments. Statistical significance was determined using a two-tailed unpaired Student's t-test: black asterisks indicate comparisons between treated cells and their corresponding untreated controls, whereas red lines and asterisks indicate comparisons between specific treated groups, including ZY vs. CFW in (a), and WT + ZY vs. *slt2*Δ + SLT2 + ZY or *rlm1*Δ + ZY in (b) (n.s., non-significant; *$P \leq 0.05$; **$P \leq 0.01$; ***$P \leq 0.001$; ****$P \leq 0.0001$). Scale bar = 10 µm.

plasma membrane proteins between the mother and daughter cells during growth, and as a gasket to sequester proteins required for completing cytokinesis and septation[55].

Regarding the fact that the septin ring failed to disassemble on the daughter side of the neck in ZY-treated cells, it is still unclear whether the separation defect is caused directly or indirectly by activation of the CWI pathway affecting septin dynamics, or whether ZY-induced damage at the septum creates a block in septin ring disassembly, ultimately preventing the cell separation machinery from functioning properly. Clarifying the underlying mechanism is difficult because septin architecture at the division site is constantly remodeled throughout the cell cycle by multiple post-translational modifications (PTMs), such as phosphorylation, and interactions with septin-associated proteins[40].

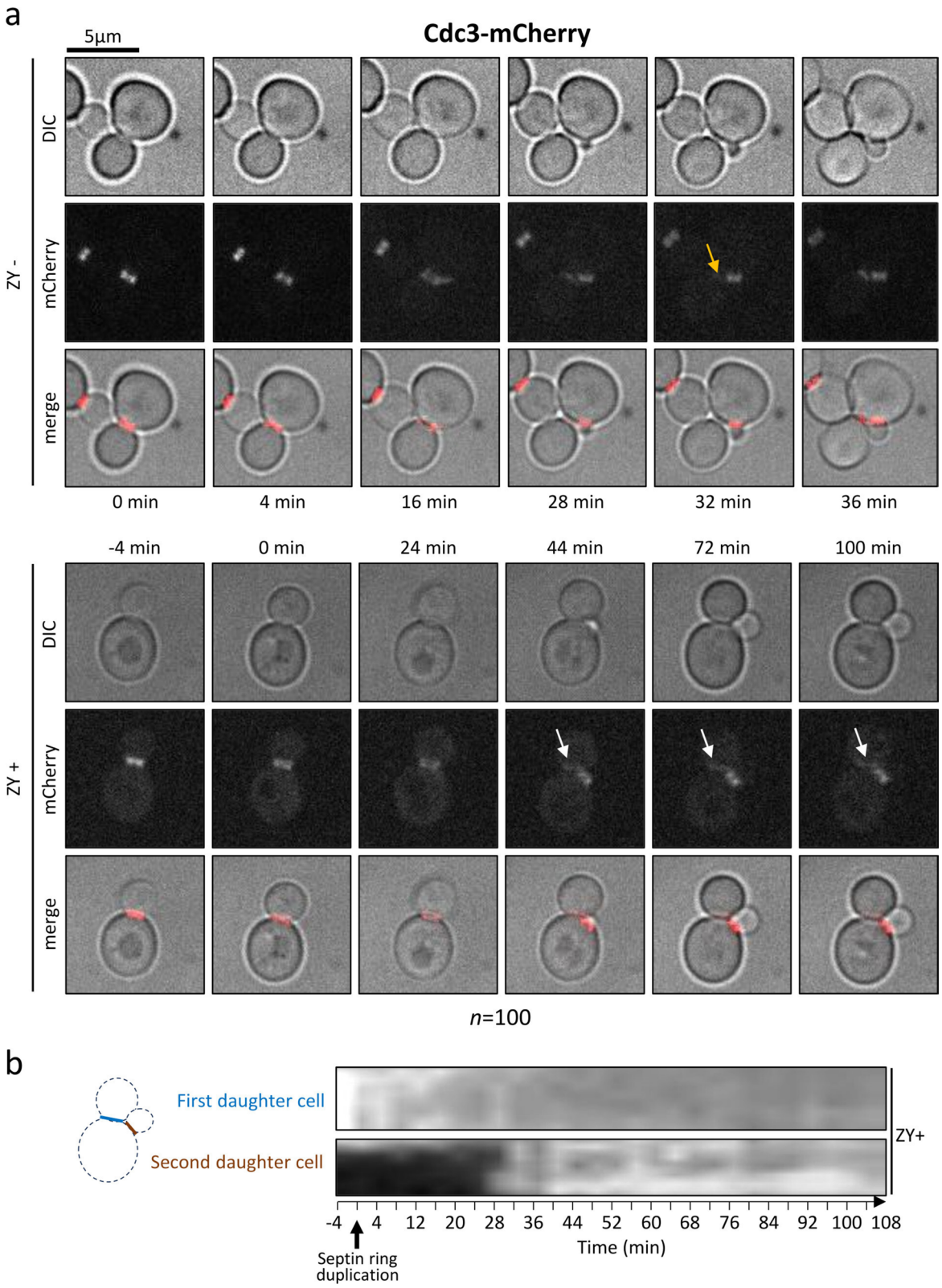
Slt2 septum localization dynamics under cell wall stress

Previous studies have shown that, in addition to its typical nucleocytoplasmic distribution, Slt2 transiently localizes to the mother-daughter septum region and sites of polarized growth in a Spa2-dependent manner[56], although its specific function at these locations remains unclear. Given that the catalytic activity of Slt2 is necessary for the cell separation delay phenotype mediated by ZY, we analyzed the timing of Slt2 localization using confocal microscopy in a strain expressing both Slt2-GFP and Cdc3-mCherry fusion proteins. As a temporal reference, time "0" was defined as the moment of septin ring duplication. Quantitative analysis of the timing and duration of Slt2-GFP localization is shown in Fig. 6. In the presence of ZY, Slt2-GFP reached the septum region of unseparated cells about 1 min earlier than in untreated conditions and remained there for nearly 3 min longer (from 4.7 to 7.4 min) (Fig. 6b). Thus, in contrast to what had been reported for *ptc1*Δ cells incubated at 38 °C, where Slt2 was not found to be abnormally retained on the daughter-cell side of the septum in multibudded *ptc1*Δ cells[49], our quantitative time-resolved imaging showed that acute cell wall stress mediated by ZY treatment prolongs Slt2 residence at the neck by approximately 3 min (1.57-fold over untreated control) and this difference is clearly seen in the kymographs shown in Fig. 6c. Although the exact significance of this altered timing remains unclear, it may be associated with persistent daughter-side septin structures, altered septin splitting dynamics, and the observed delay in cell separation. Slt2 is known to participate in a wide range of cellular processes through an expanding repertoire of substrates[57]. In this context, potential Slt2 substrates at the yeast bud neck could mediate the morphogenetic changes caused by ZY-induced stress. Future studies will aim to identify the factors responsible for the multibudded phenotype through a genome-wide phenotypic screen.

Additionally, analysis of Chs3, the catalytic subunit of chitin synthase III and the main enzyme responsible for chitin synthesis in yeast[45], showed a localization pattern under ZY stress similar to that of Slt2. Specifically, Chs3 arrived earlier at the septum (−2 min compared to untreated cells) and departed slightly later (+4 min) (Fig. 7). This aligns with the known transcriptional activation of *CHS3* by the MAPK Slt2 under cell wall stress conditions[58], as well as with the increased chitin deposition in the chitin ring at the septum previously shown (Fig. 2).

Contribution of the cell separation machinery to the multibudded phenotype

Once the septum is formed, the cell's integrity is preserved during the separation process. A key aspect of mother-daughter cell separation is the well-established asymmetric localization of the transcription factor Ace2 to the daughter nucleus following mitosis[59]. This process is regulated by the RAM signaling pathway, which includes the Cbk1 kinase and its target Ace2. For complete cell separation to occur, PS and part of the SS must be degraded by chitinases and glucanases[34,35] that are induced as part of the daughter-specific G1 transcriptional program activated by Ace2[32]. To determine whether the cell separation defect observed after ZY treatment could result from alterations in the expression of the genes encoding these hydrolases, we first analyzed the kinetics of nuclear Ace2 accumulation in cells growing in the presence or absence of ZY. We used a yeast strain expressing Ace2-GFP and Cdc3-mCherry from their endogenous loci under the control of their native promoters. The septin marker Cdc3-mCherry again served as a cell cycle "clock". As shown in Fig. 8a, time-lapse confocal microscopy revealed no significant difference in the timing of Ace2-GFP detection in cells exhibiting the cell separation



delay phenotype compared to wild-type cells (fluorescence signal observed at approximately − 7.5 min), nor in its residence time (+ 25.4 min). These values are consistent with previously reported data[60]. Similarly, cell separation defects exhibited by *ptc1*Δ mutants are not due to a failure of RAM pathway activation, suggesting that events downstream of Ace2 entry into the nucleus underlie these alterations.

To further evaluate whether Ace2-driven transcription might be impacted beyond its correct localization, we measured mRNA levels of a representative set of Ace2-regulated genes (*CTS1*, *DSE2*, *DSE4*, and *EGT2*) throughout the cell cycle. Quantitative PCR (RT-qPCR) was performed on samples from wild-type cells synchronized in G1 phase with α-factor and then released into fresh medium with or without ZY. As shown in Fig. 8c, the expression

◀**Fig. 5**. Septin dynamics are altered in multibudded cells. **(a)** Time-lapse images (DIC and confocal fluorescence microscopy) of individual cells expressing the Cdc3-mCherry fusion protein were acquired using a microfluidic platform during growth in either the presence or absence of ZY (see Methods for details). Single-cell data were aligned over time based on septin ring splitting, designated as time zero. Cell montages were generated from selected frames of the time-lapse series taken at 4-minute intervals. The row labeled "merge" shows combined images of the mCherry (red) and DIC (grey) channels. In control cells, the orange arrow indicates the transient disappearance of the Cdc3 ring from the bud neck. Conversely, in ZY-treated (multibudded) cells, the white arrows highlight the persistent localization of the Cdc3-mCherry signal on the side of the bud neck of the older daughter cell over an extended period. Representative time-lapse microscopy experiments are shown. This persistent mislocalization phenotype was observed in 100% of the cells analyzed ($n = 100$), as indicated in the bottom panel. Scale bar = 5 µm. **(b)** Kymographs illustrating the mislocalized septin structure after septin ring duplication (t = 0) in two subsequent daughter ZY+ cells. The schematic yeast cell indicates the two daughter cells used to measure fluorescence intensity. The kymographs track septin in the first daughter cell (top kymograph) and the second daughter cell (bottom kymograph). Kymographs were generated from time-lapse images acquired at 4-minute intervals.

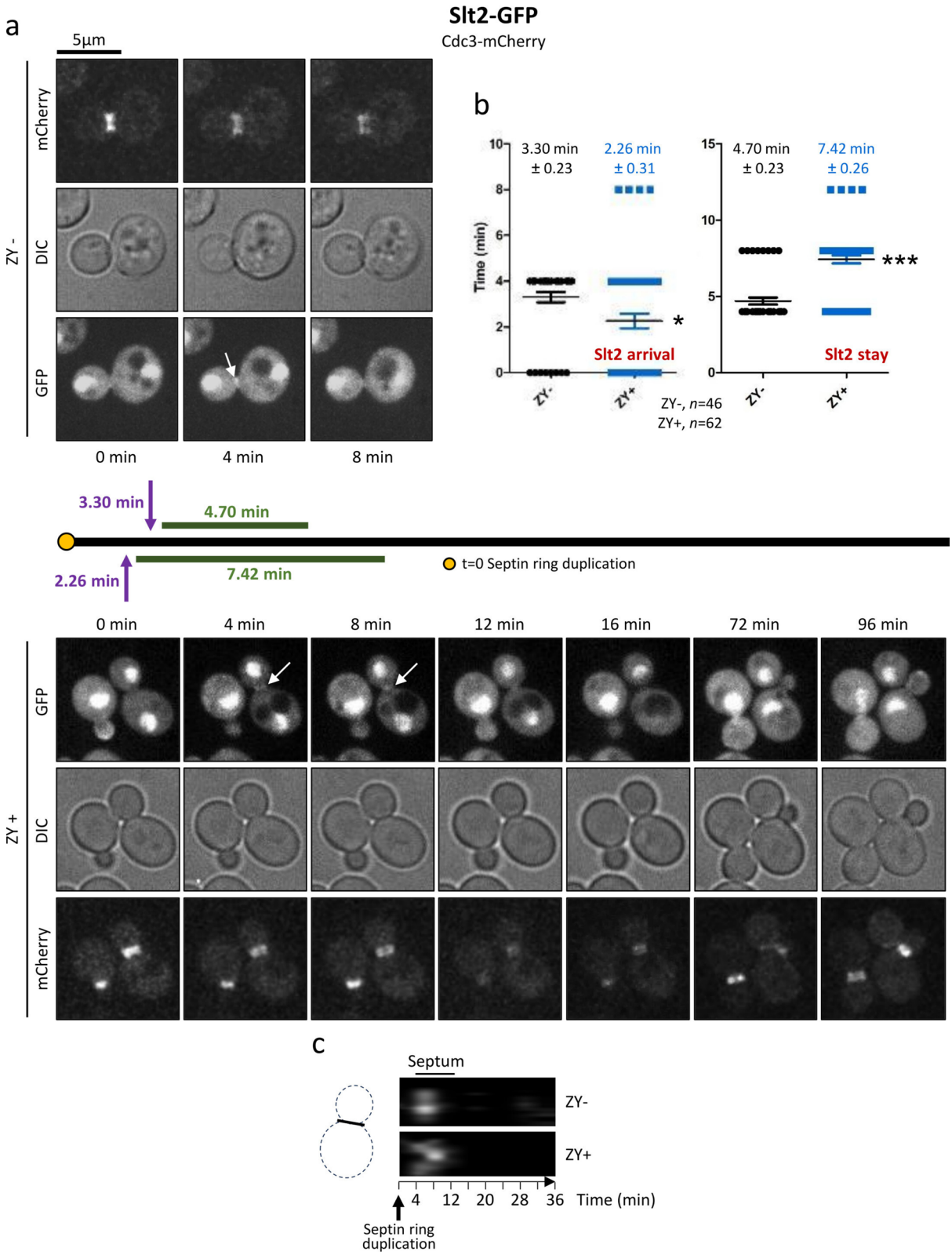
profiles of these genes were similar under both conditions. Although no significant differences in overall mRNA levels were detected between WT ± ZY, the curves in ZY-treated cells showed a slight rightward shift, indicating a delay in transcript accumulation rather than a change in expression amplitude. This pattern is consistent with a modest alteration in the kinetics of transcriptional activation rather than in the total transcriptional output. This effect does not appear to stem from major changes in the spatiotemporal regulation of Ace2, suggesting instead the possible involvement of additional regulatory mechanisms, such as chromatin remodeling or co-regulator activity, that could influence the timing of transcription. In any case, no significant repression of the Ace2-mediated transcriptional program could account for the separation defect.

At this time, we hypothesized that the separation defect was due to a failure in Cts1 (the main endochitinase responsible for cell separation[34]) transport and/or secretion. Brace et al.[36] reported that transcription of Cts1 is not grossly affected upon failed septation in the absence of Inn1, but a significant block in Cts1 secretion occurs. These authors suggested that Cbk1 induces Cts1 secretion independently of its role in *CTS1* expression and that Cbk1 plays a role in Cts1 trafficking (vesicle transport and/or membrane fusion). In a more recent work, Foltman et al.[37] described a mechanism by which the MEN kinase Cdc15 and TORC1 play opposing roles in the control of cell separation. TORC1 blocks cell separation by promoting Cbk1 phosphorylation, whereas Cdc15 prevents that inhibition and allows cells to separate. As a consequence, *cdc15-2* cells exhibit a cell separation defect at 37 °C that is rescued by inactivation of TORC1 with rapamycin. Interestingly, Cts1 is localized to the site of division at the end of the cell cycle in this mutant but cannot promote cell separation in the absence of rapamycin, as a consequence of a problem in the fusion of Cts1-containing vesicles into the plasma membrane, which could explain the cell separation defect associated with *cdc15-2* cells.

Next, we examined the localization kinetics of Cts1. Using confocal microscopy, we tracked its cellular localization over time in both the presence and absence of ZY in a strain bearing a Cts1-GFP fusion integrated at its genomic locus. This strain also includes the mRuby2-Tub1 and Mlc2-mApple fusions, which serve as a cell-cycle marker and a "clock" for reliably comparing the accumulation kinetics of different proteins of interest. In the absence of stress, the residence time of Cts1 at the septum matched previous reports, ranging from + 12 min to over 80 minutes[60] (Fig. 9). In contrast, upon ZY treatment, cells displaying the separation-delay phenotype showed a ~ 9 min lag in Cts1 arrival at the bud neck (Fig. 9). Thus, as observed in *cdc15-2* cells, and in contrast to the absence of Cts1 localization at the septum of multibudded *ptc1*Δ cells[49], acute cell wall stress mediated by ZY accumulates Cts1 at the division site in WT large budded cells, although the timing of Cts1 localization is altered. It is worth noting that the results from Gonzalez-Rubio et al.[49] do not come from studies that analyze cells over time, which precludes a direct comparison with our findings regarding Cts1 localization. The delayed arrival of Cts1 at the septum that we detected may be associated with the transitory separation delay, although we cannot rule out that the shift in its expression profile under zymolyase treatment (Fig. 8c) may also contribute to its delayed recruitment. However, as shown in Fig. 9, the fluorescent signal from the Cts1-GFP fusion protein is increased in ZY-treated cells (see the intensity in the kymographs included in this figure), suggesting that the separation phenotype is not due to insufficient levels of Cts1. Therefore, these data indicate that the delay in Cts1 arrival at the bud neck is not due to a substantial reduction in protein abundance. Instead, this effect is more plausibly explained by alterations in the intracellular trafficking of this protein. Despite its prolonged presence in the septal region (Fig. 9), we cannot rule out the possibility that Cts1 activity in the septal region may be downregulated to prevent cell wall degradation before cells adapt to cell wall injury, though further research will be necessary to confirm this.

The defective cellular process must be either a failure in the transport of secretory vesicles to the site of division and/or the fusion of these vesicles to the plasma membrane. In agreement with the first possibility, notably, we frequently observed (95.5% of cells, $n = 45$) cytoplasmic structures corresponding to Cts1-GFP accumulations in daughter cells exhibiting the separation phenotype (Fig. 9 and Fig. S4), which suggests that acute cell wall stress affects the spatiotemporal localization and transport of Cts1. This phenomenon may be functionally linked to the blockage of septum degradation and, consequently, cell separation after ZY treatment. Identifying the specific nature of these trafficking intermediates remains an objective for future research.

Concerning Cts1 transport mechanisms, Cbk1 induces Cts1 secretion independently of Cbk1's role in controlling *CTS1* expression through Ace2[36]. Moreover, the requirement for the exocyst in promoting Cts1 secretion in budding yeast is now supported by the work of Foltman et al.[37], who identified Sec3 as a Cbk1 target



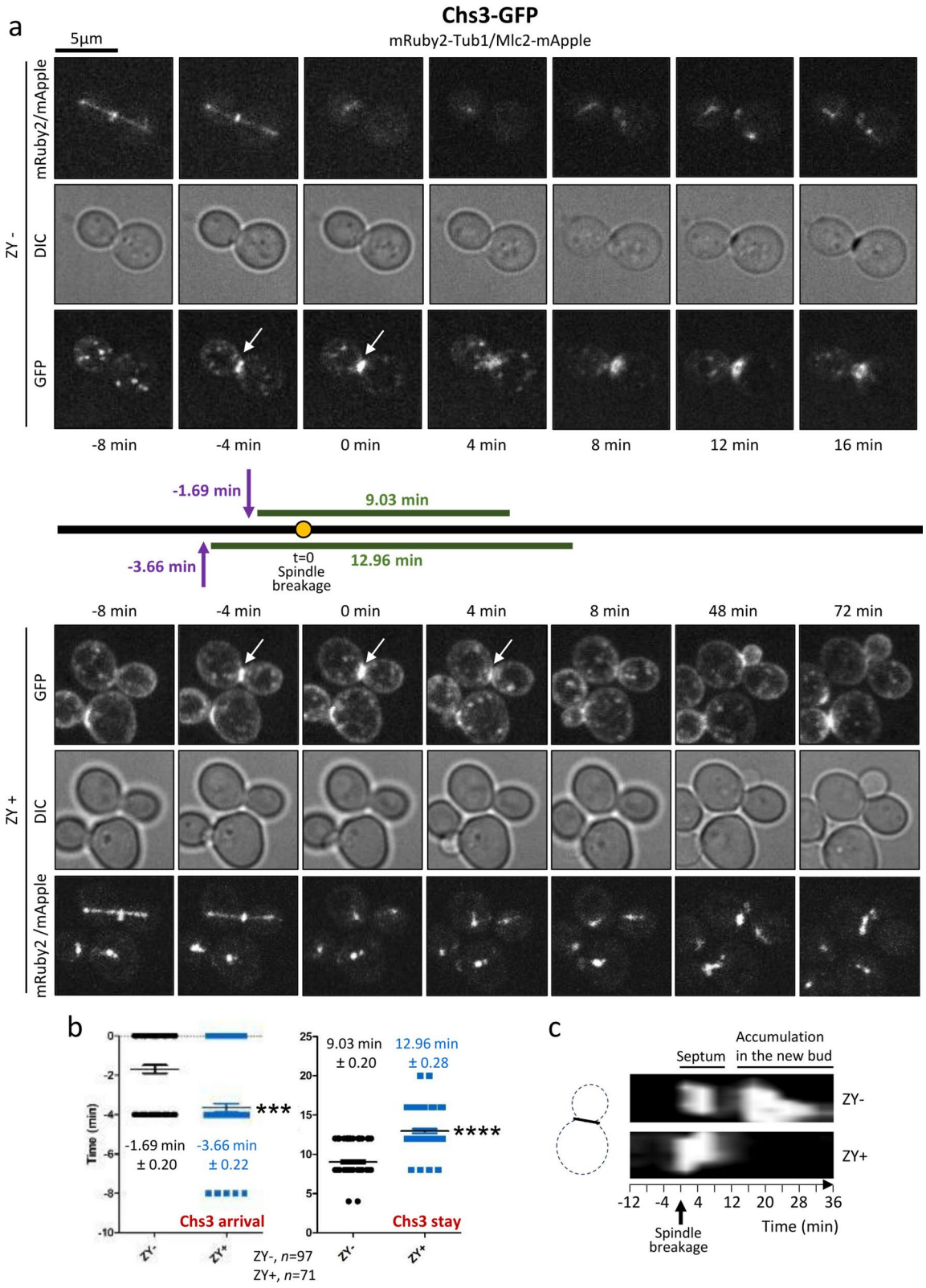
and showed that TORC1-dependent regulation of Cbk1 can affect the Sec3/exocyst-SNARE axis that promotes fusion of vesicles carrying cell separation hydrolases. To further explore the role of intracellular transport systems in the defect in Cts1 localization caused by cell wall stress, we analyzed the localization kinetics of Exo84-GFP (a subunit of the exocyst complex) and the type-V myosin Myo2-GFP. The exocyst complex mediates the tethering of secretory vesicles to the plasma membrane prior to fusion mediated by soluble N-ethylmaleimide-sensitive factor attachment protein receptors (SNAREs). The assembled exocyst subunits Sec5, Sec6, Sec8, Sec10, Sec15, Exo70 and Exo84 arrive at the yeast daughter cell plasma membrane via the secretory vesicles. There, they interact with Sec3, another component of the exocyst complex that mediates vesicle tethering during exocytosis

◀**Fig. 6**. Localization pattern of Slt2 in cells with the separation delay phenotype. **(a)** Time-lapse images (DIC and confocal fluorescence microscopy) of individual cells co-expressing Slt2-GFP and Cdc3-mCherry fusion proteins were acquired using a microfluidic platform during incubation with or without ZY (see Methods for details). Single-cell data were time-aligned to the moment of Cdc3 septin ring duplication as time zero. Cell montages were assembled from selected frames of the time-lapse series captured at 4-minute intervals. Representative time-lapse microscopy experiments are shown. White arrows in the micrographs indicate Slt2-GFP localization. Colored lines denote specific events over the time course: purple lines and numbers mark the time of Slt2-GFP arrival at the septum, while green lines and numbers indicate how long it remains there. Scale bar = 5 µm. **(b)** Quantitative analysis of the timing and duration of Slt2-GFP localization is presented in scatter plots. Each dot represents an individual cell ($n = 46$ for ZY-; $n = 62$ for ZY+), with horizontal bars and numerical values indicating the mean ± SEM. Statistical significance was determined using a two-tailed unpaired Student's t-test, comparing ZY+ with no treatment ($^{*}P \leq 0.05$; $^{***}P \leq 0.001$). **(c)** Kymographs showing Slt2-GFP accumulation at the septum of the emerging bud relative to septin ring duplication (t = 0) in ZY − and ZY+ cells. Kymographs were generated from time-lapse images acquired at 4-minute intervals. The schematic yeast cell indicates the septal region used for fluorescence intensity measurements.

and interacts with Sso1/2 to promote the t-SNARE complex assembly and stimulation of membrane fusion[38,61]. In budding yeast, Myo2 moves secretory vesicles along actin cables from the post-Golgi network to specific areas of the plasma membrane. The exocyst complex, in turn, helps tethering post-Golgi transport vesicles to sites of polarized growth on the plasma membrane, such as the tip of the growing bud and, during cytokinesis, at the mother-bud neck[38]. Using confocal fluorescence microscopy, we tracked the temporal localization pattern of both proteins, Exo84-GFP and Myo2-GFP, in individual cells. Under non-stress conditions, both proteins showed similar dynamics, consistent with previously published data[60]. They appeared in the septum area approximately 3–4 min before spindle breakage and remained there for about 27 min (Exo84 data are in Fig. 9, and Myo2 data in Fig. S5). Notably, in the presence of ZY, the residence time of both proteins at the septum was significantly reduced by 8 min. These findings suggest that ZY affects the timing of Exo84 and Myo2 localization similarly, confirming that they participate in the same intracellular trafficking pathway. The delayed arrival of Cts1 at the septum, as noted earlier, combined with the shorter residence time of Exo84 and Myo2, may decouple the localization of these proteins. Specifically, in control cells, Cts1, Exo84, and Myo2 colocalize at the septum for approximately 12 min. However, after ZY treatment, Cts1 appears in the septal region ~ 5 min after Exo84 and Myo2 are no longer detectable (Fig. 9 and Fig. S5). This observation is consistent with a defect in the coordination of Cts1 delivery with the exocytic machinery, but does not establish whether reduced Exo84/Myo2 residence causes delayed Cts1 localization or whether both events are parallel consequences of cell wall stress. Foltman et al.[37] reported that *cdc15-2* cells are able to transport Cts1 (secretory vesicle transport mediated by the exocyst components Sec8 and Sec3 is not defective in this mutant), but they may have a problem with the fusion of Cts1-containing vesicles with the plasma membrane, which could explain the cell separation defect associated with this mutant. They determined that Cbk1 phosphorylates Sec3 to induce the interaction between t-SNARE components Sso1/2 and Sec9 to drive fusion of secretory vesicles into the plasma membrane, and this step is blocked by TORC1. Although we cannot rule out that ZY mediated cell wall stress also activates a similar mechanism to block the fusion of secretory vesicles transporting hydrolases to the plasma membrane, our data, in contrast with the model established with the *cdc15-2* mutant, are consistent with altered coordination of Cts1 delivery with the secretory/exocytic machinery during ZY-mediated cell wall stress.

Highlighting the significance of Cts1 in cell separation, the ECO pathway prevents separation processes until septation is successfully completed[36]. A key element of this checkpoint is the Fir1 protein, which inhibits the Cbk1 protein kinase, thereby preventing Cts1 secretion when septation fails. Under these conditions, removing *FIR1* restores Cts1 secretion. Regarding the multibudded phenotype caused by ZY, we have not observed significant differences between the WT strain and the *fir1*Δ mutant. This result argues against a major role for Fir1-dependent ECO signaling in the ZY-induced multibudded phenotype under our conditions and with the possibility previously suggested of Fir1 being a target of the MAPK Slt2 and the CWI pathway[36,49]. However, because only *fir1*Δ was tested and Cts1 trafficking was not examined in this background under ZY treatment, we cannot rule out the possibility that ECO-like controls, partial redundancy, or other Cbk1-dependent regulatory mechanisms contribute to the response. One possible explanation is that, in the ZY-induced cell-separation phenotype, septation remains largely intact, thereby preventing the canonical Fir1-dependent ECO pathway from being triggered. In any case, since the ECO pathway monitors septation status through Fir1/Cbk1, and the CWI pathway monitors cell wall integrity through Slt2, these pathways may converge, directly or indirectly, on the timing and localization of Cts1 at the division site, making Cts1 delivery a key decision point in the coordination of cytokinesis, cell wall integrity, and cell separation.

Our data should therefore be interpreted in the context of previously described post-transcriptional control of Cts1 secretion. Brace et al. showed that ECO can inhibit Cbk1-dependent Cts1 secretion independently of Cbk1's transcriptional activation of Ace2 targets[36], and Foltman et al. demonstrated that TORC1 negatively regulates Cbk1 to control cell separation through Sec3/exocyst-SNARE-mediated membrane fusion[37]. In addition, González-Rubio et al. connected sustained Slt2 activity in *ptc1Δ* cells with reduced TORC1-Sch9 signaling and defective Cts1 localization despite normal Ace2 nuclear accumulation[49]. The last two works relate TORC1 signaling to cell separation, but apparently through different mechanisms. Whereas Foltman et al.[37] showed that TORC1 blocks the separation of cells following cytokinesis, a process which is reverted by the addition of rapamycin, Gonzalez-Rubio et al.[49] showed that Slt2 kinase activity inhibits signaling through the Sch9 branch of the TORC1 pathway in *ptc1*Δ cells. Although a single mechanism involving both TORC1 and



CWI pathways to regulate cell separation under cell wall stress is not readily apparent, our findings related to the Exo84/Myo2/Cts1 decoupling are consistent with the possibility that acute ZY-induced activation of Slt2 may ultimately impinge on the established Cbk1-exocyst-Cts1 secretion layer, either directly or through TORC1-related signaling, even though we have not directly assayed Cbk1 or Sec3. This model remains a hypothesis to be tested.

Since excessive chitinase and glucanase activities might disrupt cell wall integrity, their timing and localization during morphogenetic events are crucial. Overall, our findings suggest that the temporary delay in mother-daughter cell separation caused by cell wall stress could result from two combined effects: the lack of coordination

◀**Fig. 7**. Examination of Chs3 localization dynamics in cells with delayed cytokinesis. **(a)** Time-lapse images (DIC and confocal fluorescence microscopy) of individual cells co-expressing Chs3-GFP and mRuby2-Tub1/Mlc2-mApple fusion proteins were captured using a microfluidic platform (see Methods for details) during incubation in the presence or absence of ZY. All single-cell data were aligned in time to the disassembly of the mitotic spindle, designated as time zero. Cell montages were assembled from selected frames of time-lapse series acquired every 4 min. Representative time-lapse microscopy experiments are shown. White arrows in the images indicate the location of Chs3-GFP. Colored lines and numbers denote specific events during the time course: purple indicates when Chs3-GFP arrives at the septum, and green shows how long it remains there. Scale bar = 5 µm. **(b)** Quantitative analysis of the timing and duration of Chs3-GFP localization is presented in scatter plots. Each dot represents an individual cell ($n = 97$ for ZY-; $n = 71$ for ZY+), with horizontal bars and numerical values indicating the mean ± SEM. Statistical significance was determined using a two-tailed unpaired Student's t-test, comparing ZY+ with no treatment (***$P \leq 0.001$; ****$P \leq 0.0001$). **(c)** Kymographs showing Chs3-GFP accumulation at the septum of the emerging bud relative to mitotic spindle disassembly (time 0) in ZY – and ZY+ cells. Kymographs were generated from time-lapse images acquired at 4-min intervals. The schematic yeast cell indicates the septal region used for fluorescence intensity measurements.

in secreting these enzymes, which are needed for the proper septum degradation and cell separation, and the increase in the thickness of the SS in daughter cells caused by cell wall stress. Besides increasing thickness, this SS may also have a different structure and composition, making it more resistant to degradation. The broader significance of our findings is that the trafficking of Cts1, and likely other separation proteins, in yeast is precisely regulated to manage cell wall stress. This regulation involves the essential participation of the Cell Wall Integrity (CWI) pathway in coordination with septin assembly, temporarily preventing cell separation when cell wall integrity is compromised.

Taken together, the results of this study highlight multiple coordinated mechanisms that aim to preserve cellular homeostasis when the cell wall is impaired. In this context, it has been reported that in yeast under ER stress conditions, the MAPK Slt2 physically interacts with exocyst subunits Sec6 and Exo84, and also indirectly participates in septin dynamics[62]. Additionally, in the fission yeast *Schizosaccharomyces pombe*, septins have been shown to regulate exocyst localization through direct physical interactions[63]. Additionally, the CWI pathway is activated in polarized growth phases, such as budding and cytokinesis. Therefore, the multibudded phenotype described in this work, resulting from acute cell wall stress, may represent an amplification of a normal CWI-mediated surveillance mechanism. The transient, recoverable nature of the phenotype suggests a tunable checkpoint that may operate throughout cytokinesis, with its effects becoming evident only when cell wall integrity is compromised. This framing would provide additional breadth and connect the stress response to underlying cell biology, although further work will be required to determine if this mechanism operates during unperturbed cytokinesis.

Remarkably, all these findings pave the way for future research focused on understanding the molecular mechanisms that control cell separation and their interactions under conditions of cell wall stress.

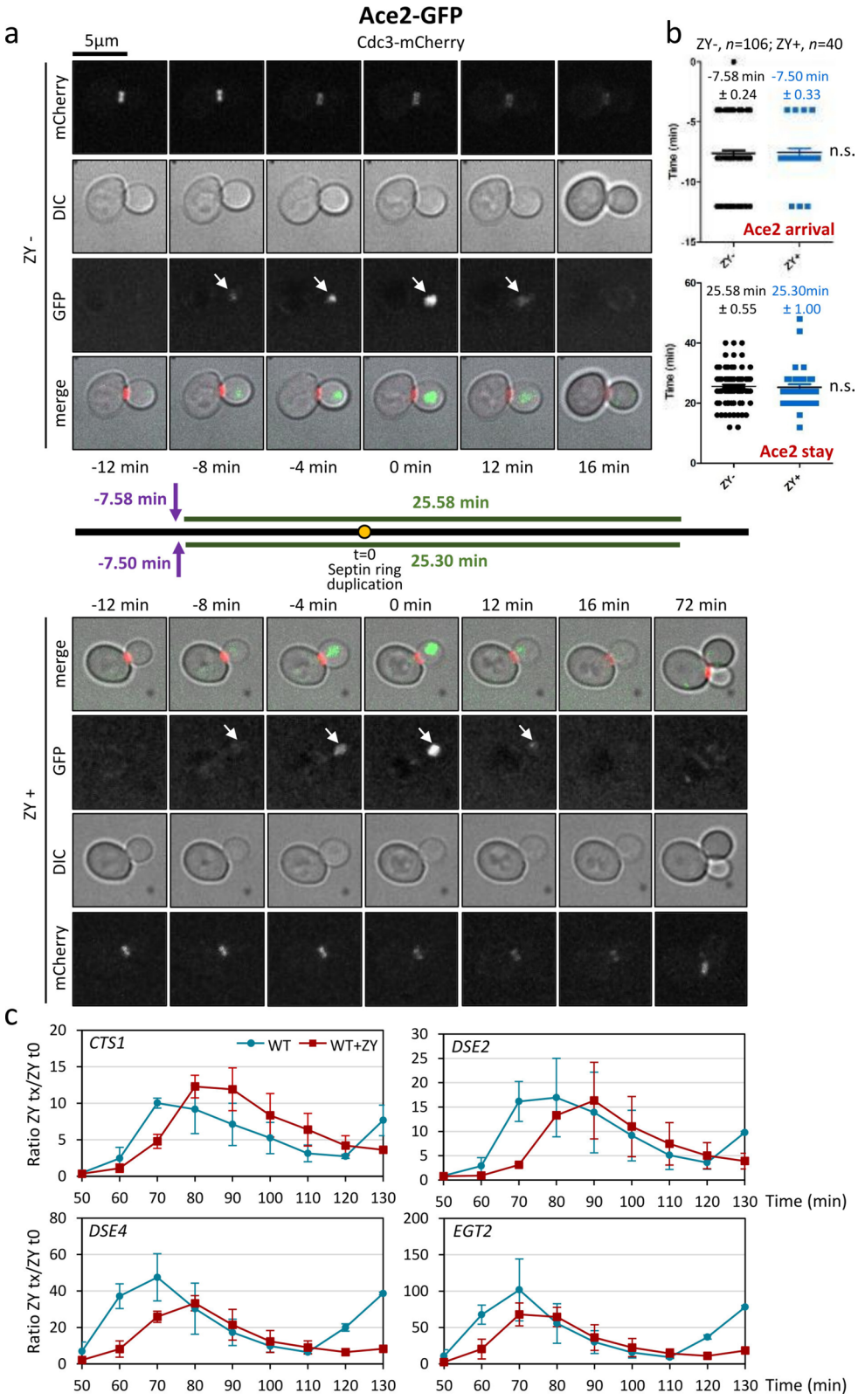
Methods

Yeast strains, plasmids, and growth conditions

Phenotypic and transcriptomic analyses were performed using the *S. cerevisiae* wild-type strain BY4741 (*MAT*a; *his3Δ1*, *leu2Δ0*, *met15Δ0*, *ura3Δ0*). The mutant strains *slt2*Δ, *rlm1*Δ, and *sho1*Δ were obtained from the European *Saccharomyces cerevisiae* Archive for Functional Analysis (EUROSCARF, Scientific Research and Development GmbH, Oberursel, Germany). The *whi7*Δ and *fir1*Δ deletion strains were created using the PCR-based SFH method[64,65], by replacing each gene with the *HIS3MX6* and *KanMX4* resistance cassettes, respectively. For fluorescence microscopy-based kinetic analyses, we used the wild-type strain YEF473A (S288c background), expressing *TUB1::HPH-pHIS3-mRuby2-TUB1*, *MLC2-mApple-URA3MX*, additionally carrying GFP-tagged versions of Chs3, Cts1, Exo84, or Myo2 expressed from their endogenous loci under the control of their native promoters. These strains were generously provided by Erfei Bi (Department of Cell and Developmental Biology, Perelman School of Medicine, University of Pennsylvania, Philadelphia, PA, USA)[60]. The wild-type strain expressing the fusion Cdc3-mCherry and yeast strains co-expressing Cdc3-mCherry with either Slt2-GFP or Ace2-GFPwere constructed by transforming the plasmid YIn211-CDC3-mCherry[66] digested with *Bgl*II for its integration at the genomic *CDC3* locus. To evaluate the temporal pattern of expression of the proteins Clb3 and Sic1, we used the strain YAN48[67] provided by Francesc Posas (IRB Barcelona - Institute for Research in Biomedicine, Barcelona, Spain). This strain is a wild-type BY4741 carrying a genome-integrated TAP-tagged version of Clb3 and Sic1 simultaneously.

Plasmids based on the pRS315 backbone encoding various *SLT2*/*MPK1* alleles, including TA/YF (p2190), K54R (p2193), and the wild-type gene (p2188), were described previously[19].

Cells were routinely grown overnight in yeast extract peptone dextrose (YPD) medium (1% yeast extract (Condalab, Madrid, Spain), 2% peptone (Condalab, Madrid, Spain), and 2% glucose (Thermo Fisher Scientific, Waltham, MA, USA) or, for plasmid-bearing strains, in synthetic defined (SD) medium (0.17% yeast nitrogen base, 0.5% ammonium sulfate, 2% glucose) supplemented with the appropriate amino acids. Cultures were incubated at 24 °C with shaking at 180 rpm until reaching an optical density at 600 nm (OD_{600}) of 0.6–0.8. All cultures were subsequently diluted to an OD_{600} of 0.2 in fresh YPD and grown for an additional 2 h at 28 °C before being divided into two portions. One portion continued growing under the same conditions (untreated control), while the other was treated with zymolyase 100 T from *Arthrobacter luteus* (ZY) (Immuno™; MP Biomedicals, CA, USA) at a final concentration of 0.8 U/ml. Cells were harvested at the indicated time points and processed



according to the specific experimental protocols. Cells transformed with plasmids were grown overnight in SD-Leu medium at 24 °C, and then refreshed in YPD at 28 °C for 2 h prior to treatment or not with ZY.

Additional compounds used in this study included Calcofluor White (CFW; Fluorescent Brightener 28, Sigma-Aldrich, Merck, Darmstadt, Germany), KCl (Sigma-Aldrich, Merck, Darmstadt, Germany), hydrogen peroxide (PanReac AppliChem, Castellar del Vallès, Barcelona, Spain), tunicamycin (Sigma-Aldrich, Merck, Darmstadt, Germany), and sorbitol (PanReac AppliChem, Castellar del Vallès, Barcelona, Spain).

◀**Fig. 8**. Analysis of Ace2 localization and expression of Ace2 target genes in cells with a delayed separation phenotype. **(a)** Time-lapse images of individual cells co-expressing Ace2-GFP and Cdc3-mCherry were obtained using a microfluidic platform (see Methods for details) during incubation in the presence or absence of ZY. Single-cell data were time-aligned to the Cdc3 septin ring splitting event, set as time zero. Cell montages were created from selected frames of the time-lapse series captured at 4-minute intervals. Representative time-lapse microscopy experiments are shown. The row labeled "merge" shows combined images of the GFP (green), mCherry (red), and DIC (grey) channels. White arrows indicate Ace2-GFP localization. Colored lines and numbers represent specific events during the time course: purple marks the time of Ace2-GFP arrival at the septum, and green shows its persistence. Scale bar = 5 µm. **(b)** Quantitative analysis of the timing and duration of Ace2-GFP localization is presented in scatter plots. Each dot represents an individual cell ($n = 106$ for ZY-; $n = 40$ for ZY+), with horizontal bars and numerical values indicating the mean ± SEM. Statistical significance was determined using a two-tailed unpaired Student's t-test, comparing ZY+ with no treatment (n.s., not significant; $P > 0.05$). **(c)** The expression kinetics of *CTS1*, *DSE2*, *DSE4*, and *EGT2* mRNAs were analyzed by RT-qPCR in wild-type (WT) cultures synchronized in G1 phase with α-factor. After release, cells were transferred to fresh medium with or without 0.8 U/mL ZY. Samples were collected at the indicated time points. Expression levels are shown relative to time zero (immediately before the addition of ZY). The graphs show the mean value and SD of the relative expression levels obtained from two independent experiments.

Cell synchronization

Yeast cell synchronization was performed according to protocols previously described by Manukyan et al.[68] and Juanes[69].

Briefly, for synchronization in the G1 phase and subsequent release, yeast cells were grown to the exponential phase ($OD_{600} \approx 0.25$) at 24 °C. Cells were then harvested by centrifugation, the supernatant was discarded, and the pellet was washed twice with sterile water. After a final centrifugation step to remove residual water, the cells were resuspended in prewarmed YPD medium at 28 °C containing 10 µg/mL alpha-factor (SP-AFMP-10, Innovagen, Lund, Sweden). Cultures were incubated for approximately 2.5 h until > 95% of cells displayed the characteristic pear-shaped morphology under the microscope, indicative of G1 arrest. To release the cells from arrest, they were pelleted, washed twice with sterile water, and resuspended in YPD medium supplemented with 50 µg/mL of pronase (Roche Diagnostics GmbH, Mannheim, Germany). The culture was then divided into two: one for the untreated control and the other for the experimental treatment, as required. Samples were collected at the indicated time points and either examined under a microscope to determine the budding index or processed for downstream experimental procedures.

For S phase synchronization (large-budded doublets), hydroxyurea (HU; A10831, Thermo Fisher Scientific, Waltham, MA, USA) was used to arrest cells. Cultures were grown to the exponential phase ($OD_{600} \approx 0.25$) at 30 °C, and HU was added directly to a final concentration of 0.2 M. Cells were incubated at 30 °C for 3.5 h, until more than 95% of the population displayed large buds. To release the arrest, cells were harvested by centrifugation and washed twice with prewarmed YPD. Cultures were then divided and processed as described above.

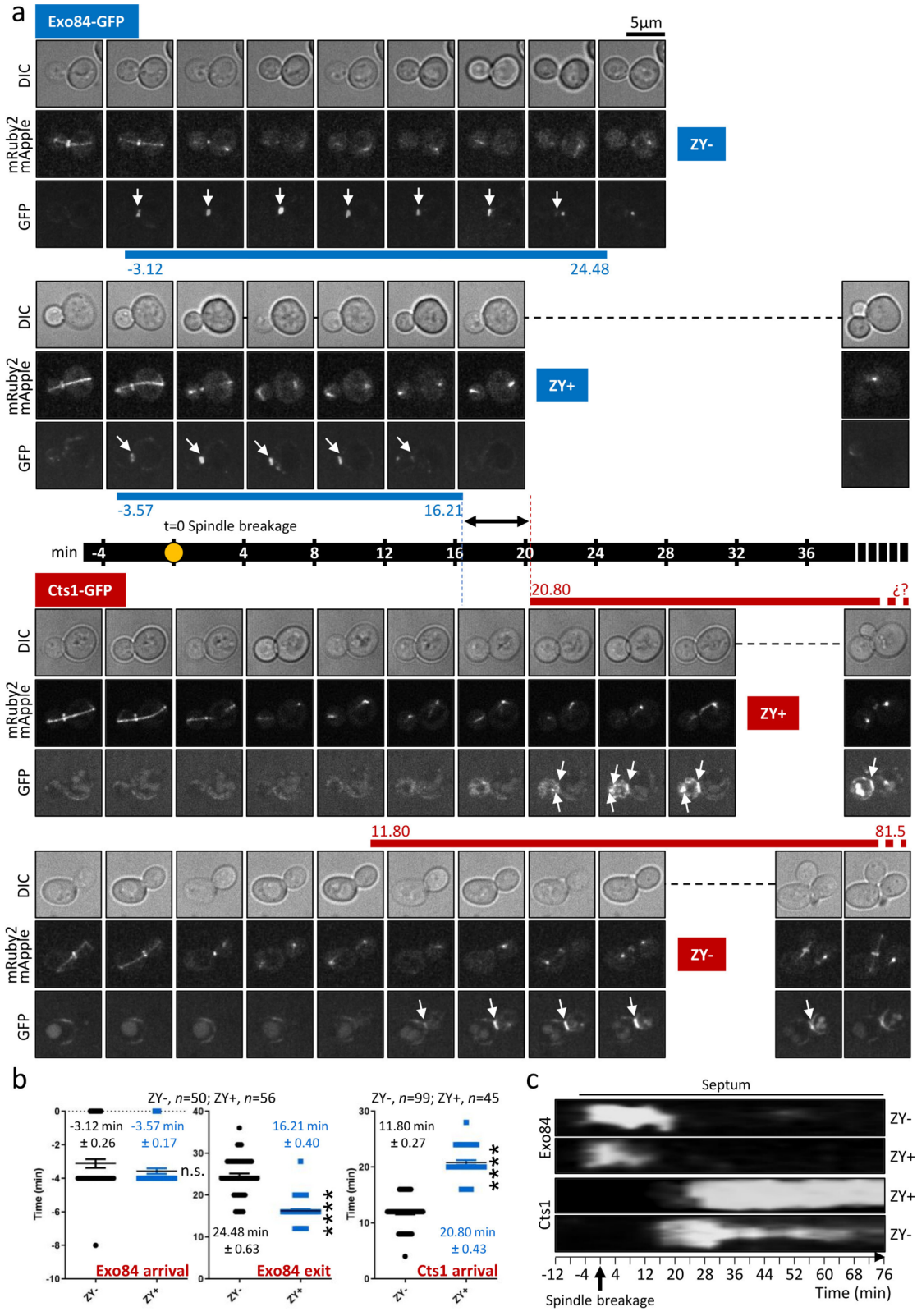
Microscopy, imaging, and data analysis

The budding index was determined by differential interference contrast (DIC) microscopy on exponentially growing cultures and during time-course experiments. Usually, all cell counts were obtained from at least three independent experiments, each analyzing more than 100 cells.

Fluorescently stained yeast cells were examined using an Eclipse TE2000 inverted microscope (Nikon, Tokyo, Japan) equipped for both fluorescence and DIC imaging. Digital images were captured with an Orca C4742-95-12ER CCD camera (Hamamatsu Photonics, Shizuoka, Japan) and processed using HCImage software (Hamamatsu Photonics, Shizuoka, Japan). For CFW staining, cells were washed with cold PBS and stained in the dark with 5 µg/mL CFW (in PBS) for 10 min. For nuclear DNA staining, cells were washed once with PBS and incubated with DAPI (D9542, Sigma-Aldrich, Merck, Darmstadt, Germany) at a final concentration of 2.5 µg/mL for 5 min in PBS, followed by two additional PBS washes prior to fluorescence microscopy.

Transmission electron microscopy (TEM) was performed as previously described[70]. Briefly, 1 mL ($\sim 2 \times 10^7$ cells) of alpha-factor synchronized cultures grown in YPD at 28 °C were harvested and washed twice with PBS. Cells were fixed at 4 °C for 24 h in 500 µL of fixative solution (0.05 M sodium cacodylate buffer, pH 7.2 (Merck, Darmstadt, Germany), 2% paraformaldehyde (PanReac AppliChem, Castellar del Vallès, Barcelona, Spain), 1.5% glutaraldehyde (Sigma-Aldrich, Merck, Darmstadt, Germany). After two PBS washes, cells were treated with 1% (w/v) potassium permanganate (PanReac AppliChem, Castellar del Vallès, Barcelona, Spain) for 90 min at 4 °C under gentle agitation, then washed three times with PBS. Samples were dehydrated through an ethanol gradient (30%, 40%, 50%, 60%, 70%, 80%, 90%, and 100%, v/v; 10 min each), centrifuged to remove residual ethanol, and embedded in EMbed-812 resin (Embedding Kit, Cat. 14120, Electron Microscopy Sciences, Hatfield, PA, USA) following the manufacturer's protocol. Ultrathin sections of the solidified resin were cut, stained with uranyl acetate (PanReac AppliChem, Castellar del Vallès, Barcelona, Spain) and lead citrate (Ultrostain 2, Leica Microsystems GmbH, Wetzlar, Germany), and examined with a JEOL JEM 1010 transmission electron microscope (JEOL, Tokyo, Japan).

To measure the thickening of the secondary septum (SS) and chitin ring at the septal region, the following procedure was applied. Quantification of both parameters from TEM images was performed using the "straight-line" tool in ImageJ software. To determine SS thickness, five equidistant perpendicular lines were drawn, bounded by the less electron-dense layer corresponding to chitin (primary septum) and the more electron-dense layer corresponding to the plasma membrane. This procedure was applied to both the mother cell side



and the daughter cell side in cells treated with or without ZY. Final data were calculated as the mean value of the five measurements obtained in each case. For the assessment of chitin ring thickening, three equidistant radial lines were drawn encompassing the chitin-rich regions located at the edges of the bud neck. As in the case of SS measurements, final size values per cell were obtained by calculating the mean of the three measurements performed in each case.

Confocal fluorescence microscopy was performed using an Olympus IX81 microscope equipped with a spinning-disk confocal system and an Evolve EMCCD camera (Roper Scientific, Trenton, NJ, USA). For time-lapse imaging, a CellASIC® ONIX2 Microfluidic Platform and CellASIC® Y04C-02 microfluidic plates (Merck,

◀**Fig. 9**. Zymolyase treatment affects the timing of localization for Exo84 and Cts1. **(a)** Time-lapse fluorescence microscopy was conducted on individual cells co-expressing either Exo84-GFP or Cts1-GFP with the markers mRuby2-Tub1/Mlc2-mApple. Cells were imaged using a microfluidic platform in the presence (ZY+) or absence (ZY-) of ZY. All single-cell data were aligned to the moment of mitotic spindle disassembly (t = 0 min). Representative time-lapse microscopy experiments are shown. Black dashed lines connecting DIC images indicate gaps in the time series, corresponding to longer intervals than the standard 4-minute frame rate. White arrows in the micrographs indicate the location of the respective GFP-tagged proteins. Blue (Exo84) and red (Cts1) horizontal bars, along with numerical values, show the time at which each protein appears and disappears at the bud neck. The black double-headed arrow highlights the temporal interval between Exo84 disappearance and Cts1 arrival. Scale bar = 5 µm. **(b)** Quantitative analysis of the timing of Exo84 arrival/exit and Cts1 arrival is presented in scatter plots. Each dot represents an individual cell (*n* values for each condition are specified above the plots), with horizontal bars and numerical values indicating the mean ± SEM. Statistical significance was determined using a two-tailed unpaired Student's t-test, comparing ZY+ with no treatment (n.s., not significant; $^{****}P \leq 0.0001$). **(c)** Kymographs illustrating the accumulation of Exo84 and Cts1 at the septum relative to spindle disassembly (t = 0) in ZY- and ZY+ cells. Kymographs were generated from time-lapse sequences captured at 4-minute intervals.

Darmstadt, Germany) were used according to the manufacturer's instructions. Briefly, exponentially growing cells were loaded into the chambers at 8 psi for 5 s. Untrapped cells were removed by washing with YPD at 5 psi for 5 min. After selecting fields of interest, a continuous flow of YPD (for control experiments) or YPD supplemented with ZY (2.5 U/mL) at 2 psi was maintained throughout the experiment. The temperature was set to 28 °C. The concentration of ZY used in microfluidic experiments (2.5 U/mL) differs from that used in standard flask-based assays (0.8 U/mL). This adjustment reflects the distinct growth conditions in microfluidic chambers, which involve continuous medium flow and spatial confinement, in contrast to the agitation and aeration present in flask cultures. Under microfluidic conditions, treatment with 0.8 U/mL ZY did not reproducibly induce the multibudded phenotype at the expected frequency; therefore, a higher concentration (2.5 U/mL) was required to achieve a comparable phenotypic response. Importantly, a concentration of 2.5 U/mL remains largely sublethal for the BY4741 genetic background used in our study, as this strain is able to grow in the presence of more than 60 U/mL ZY[44,71]. Five to seven z-planes were acquired every 4 min with a step size of 0.5 µm. Images were processed using ImageJ (http://rsb.info.nih.gov/ij/) or Metamorph (Molecular Devices, San Jose, CA, USA).

Kymographs were generated using ImageJ/Fiji software to visualize the spatiotemporal dynamics of protein localization at the bud neck. For each time-lapse sequence, a representative subset of frames was selected using the 'Make Substacks' tool. A 1-pixel-wide line was traced across the septum, parallel to the division plane. The 'Reslice' command was then used to extract pixel intensities along this line for every time point. The resulting kymographs were oriented so that the x-axis represents time and the y-axis represents the spatial distribution of the signal.

Quantitative-RT-PCR assays

For gene expression experiments, total RNA was extracted and purified from 3 to 5 ml of cell culture, previously flash-frozen in liquid nitrogen, using the *Nucleospin RNA* kit (Macherey Nagel, Düren, Germany), following the manufacturer's instructions. cDNA synthesis was carried out with the *PrimeScript RT-PCR* kit (Takara Bio, Shiga, Japan) using 1 µg of total RNA. Real-time quantitative PCR (RT-qPCR) assays were perform in a *QuantStudio™ 7 Real-Time PCR System®* (Applied Biosystems, Foster, CA, USA) in a final volume of 10.2 µl containing 4 µl of a 100-fold dilution of the RT reaction, 5 µl of the *Power SYBR Green PCR Master Mix* (Roche Diagnostics GmbH, Mannheim, Germany) and 0.6 µl of each primer at 5 µM stock. For quantification, the abundance of each gene was determined relative to the standard transcript of *ACT1* for input cDNA normalization, and the relative gene expression between conditions was calculated using the $2^{-\Delta\Delta Ct}$ method[72]. Primer sequences are available upon request.

Western blot assays

Yeast cultures were synchronized in G1 phase with α-factor and then released from cell-cycle arrest, either with or without ZY as described above. At different times, culture samples were taken and processed for Western blot analyses or examined under the microscope to determine the budding index (measurements were obtained from at least 150 cells for each sample in triplicate). Total protein extracts were isolated from each sample. Lysis, collection of proteins, separation by SDS-PAGE, and transfer to nitrocellulose membranes were performed as previously described[44] using the Odyssey Infrared Imaging System (LI-COR Biosciences, Lincoln, NE, USA). The detection of Sic1-TAP and Clb3-TAP was accomplished using the polyclonal antibody anti-TAP (CAB1001, Invitrogen-Thermo Fisher Scientific, Waltham, MA, USA). To monitor protein loading, actin was detected using anti-beta actin mAb (ab170325, Abcam, Cambridge, UK). Membrane-bound immune complexes were detected by incubation with a 1:5000 dilution of an appropriate infrared dye-labeled secondary antibody: 680LT Goat anti-Mouse IgG or 800 CW Goat-anti-Rabbit IgG (LI-COR Biosciences, Lincoln, NE, USA). Bands were quantified using the program Image Lab version 6.1.0. (Bio-Rad Laboratories, Inc.). Relative amounts of the different proteins in the presence or absence of ZY were obtained after normalization of the respective bands to the loading control.

Data availability

Data and materials are available upon request to the corresponding authors.

Received: 11 December 2025; Accepted: 8 July 2026
Published online: 17 July 2026

References

1. Levin, D. E. Regulation of cell wall biogenesis in *Saccharomyces cerevisiae*: The cell wall integrity signaling pathway. *Genetics* **189**, 1145–1175. https://doi.org/10.1534/genetics.111.128264 (2011).
2. Orlean, P. Architecture and biosynthesis of the *Saccharomyces cerevisiae* cell wall. *Genetics* **192**, 775–818. https://doi.org/10.1534/genetics.112.144485 (2012).
3. Cortés, J. C. G., Curto, M. A., Carvalho, V. S. D., Pérez, P. & Ribas, J. C. The fungal cell wall as a target for the development of new antifungal therapies. *Biotechnol. Adv.* **37**107352. https://doi.org/10.1016/j.biotechadv.2019.02.008 (2019).
4. Wiederhold, N. P. The antifungal arsenal: Alternative drugs and future targets. *Int. J. Antimicrob. Agents* https://doi.org/10.1016/j.ijantimicag.2017.09.002 (2017).
5. Latgé, J. P. 30 years of battling the cell wall. *Med. Mycol.* **55**, 4–9. https://doi.org/10.1093/mmy/myw076 (2017).
6. Goldenbogen, B. et al. Dynamics of cell wall elasticity pattern shapes the cell during yeast mating morphogenesis. *Open Biol.* https://doi.org/10.1098/rsob.160136 (2016).
7. Cabib, E. & Arroyo, J. How carbohydrates sculpt cells: chemical control of morphogenesis in the yeast cell wall. *Nat. Rev. Microbiol.* **11**, 648–655. https://doi.org/10.1038/nrmicro3090 (2013).
8. Popolo, L., Gualtieri, T. & Ragni, E. The yeast cell-wall salvage pathway. *Med. Mycol.* **39** (Suppl 1), 111–121 (2001).
9. Arroyo, J., Bermejo, C., García, R. & Rodríguez-Peña, J. M. Genomics in the detection of damage in microbial systems: Cell wall stress in yeast. *Clin. Microbiol. Infect.* **15**(Suppl 1), 44–46. https://doi.org/10.1111/j.1469-0691.2008.02676.x (2009).
10. Sanz, A. B., García, R., Pavón-Vergés, M., Rodríguez-Peña, J. M. & Arroyo, J. Control of gene expression via the yeast CWI pathway. *Int. J. Mol. Sci.* https://doi.org/10.3390/ijms23031791 (2022).
11. Sanz, A. B., García, R., Rodríguez-Peña, J. M. & Arroyo, J. The CWI pathway: Regulation of the transcriptional adaptive response to cell wall stress in yeast. *J. Fungi* https://doi.org/10.3390/jof4010001 (2017).
12. Fortwendel, J. R. et al. Transcriptional regulation of chitin synthases by calcineurin controls paradoxical growth of *Aspergillus fumigatus* in response to caspofungin. *Antimicrob. Agents Chemother.* **54**, 1555–1563. https://doi.org/10.1128/AAC.00854-09 (2010).
13. Gow, N. A. R., Latgé, J. P. & Munro, C. A. The fungal cell wall: Structure, biosynthesis, and function. *Microbiol. Spectr.* https://doi.org/10.1128/microbiolspec.FUNK-0035-2016 (2017).
14. Kock, C., Dufrene, Y. F. & Heinisch, J. J. Up against the wall: is yeast cell wall integrity ensured by mechanosensing in plasma membrane microdomains? *Appl. Environ. Microbiol.* **81**, 806–811. https://doi.org/10.1128/AEM.03273-14 (2015).
15. Levin, D. E. Cell wall integrity signaling in *Saccharomyces cerevisiae*. *Microbiol. Mol. Biol. Rev.* **69**, 262–291. https://doi.org/10.1128/MMBR.69.2.262-291.2005 (2005).
16. Watanabe, Y., Irie, K. & Matsumoto, K. Yeast RLM1 encodes a serum response factor-like protein that may function downstream of the Mpk1 (Slt2) mitogen-activated protein kinase pathway. *Mol. Cell. Biol.* **15**, 5740–5749. https://doi.org/10.1128/MCB.15.10.5740 (1995).
17. Baetz, K., Moffat, J., Haynes, J., Chang, M. & Andrews, B. Transcriptional coregulation by the cell integrity mitogen-activated protein kinase Slt2 and the cell cycle regulator Swi4. *Mol. Cell. Biol.* **21**, 6515–6528. https://doi.org/10.1128/MCB.21.19.6515-6528.2001 (2001).
18. García, R., Sanz, A. B., Rodríguez-Peña, J. M., Nombela, C. & Arroyo, J. Rlm1 mediates positive autoregulatory transcriptional feedback that is essential for Slt2-dependent gene expression. *J. Cell. Sci.* **129**, 1649–1660. https://doi.org/10.1242/jcs.180190 (2016).
19. Kim, K. Y., Truman, A. W. & Levin, D. E. Yeast Mpk1 mitogen-activated protein kinase activates transcription through Swi4/Swi6 by a noncatalytic mechanism that requires upstream signal. *Mol. Cell. Biol.* **28**, 2579–2589. https://doi.org/10.1128/MCB.01795-07 (2008).
20. Quilis, I., Gomar-Alba, M. & Igual, J. C. The CWI pathway: A versatile toolbox to arrest cell-cycle progression. *J. Fungi* https://doi.org/10.3390/jof7121041 (2021).
21. Igual, J. C., Johnson, A. L. & Johnston, L. H. Coordinated regulation of gene expression by the cell cycle transcription factor Swi4 and the protein kinase C MAP kinase pathway for yeast cell integrity. *EMBO J.* **15**, 5001–5013 (1996).
22. Kim, K. Y., Truman, A. W., Caesar, S., Schlenstedt, G. & Levin, D. E. Yeast Mpk1 cell wall integrity mitogen-activated protein kinase regulates nucleocytoplasmic shuttling of the Swi6 transcriptional regulator. *Mol. Biol. Cell.* **21**, 1609–1619. https://doi.org/10.1091/mbc.e09-11-0923 (2010).
23. Méndez, E. et al. The budding yeast start repressor Whi7 differs in regulation from Whi5, emerging as a major cell cycle brake in response to stress. *J. Cell Sci.* https://doi.org/10.1242/jcs.251413 (2020).
24. Harrison, J. C., Bardes, E. S., Ohya, Y. & Lew, D. J. A role for the Pkc1p/Mpk1p kinase cascade in the morphogenesis checkpoint. *Nat. Cell Biol.* **3**, 417–420. https://doi.org/10.1038/35070104 (2001).
25. Moreno-Torres, M., Jaquenoud, M. & De Virgilio, C. TORC1 controls G1-S cell cycle transition in yeast via Mpk1 and the greatwall kinase pathway. *Nat. Commun.* **6**, 8256. https://doi.org/10.1038/ncomms9256 (2015).
26. Duch, A. et al. Multiple signaling kinases target Mrc1 to prevent genomic instability triggered by transcription-replication conflicts. *Nat. Commun.* **9**, 379. https://doi.org/10.1038/s41467-017-02756-x (2018).
27. Negishi, T. et al. The late S-phase transcription factor Hcm1 is regulated through phosphorylation by the cell wall integrity checkpoint. *Mol. Cell. Biol.* **36**, 941–953. https://doi.org/10.1128/MCB.00952-15 (2016).
28. Roncero, C., Celador, R., Sánchez, N., García, P. & Sánchez, Y. The role of the cell integrity pathway in septum assembly in yeast. *J. Fungi* https://doi.org/10.3390/jof7090729 (2021).
29. Lesage, G. & Bussey, H. Cell wall assembly in *Saccharomyces cerevisiae*. *Microbiol. Mol. Biol. Rev.* **70**, 317–343. https://doi.org/10.1128/MMBR.00038-05 (2006).
30. Weiss, E. L. Mitotic exit and separation of mother and daughter cells. *Genetics* **192**, 1165–1202. https://doi.org/10.1534/genetics.112.145516 (2012).
31. Howell, A. S. & Lew, D. J. Morphogenesis and the cell cycle. *Genetics* **190**, 51–77. https://doi.org/10.1534/genetics.111.128314 (2012).
32. Colman-Lerner, A., Chin, T. E. & Brent, R. Yeast Cbk1 and Mob2 activate daughter-specific genetic programs to induce asymmetric cell fates. *Cell* **107**, 739–750. https://doi.org/10.1016/s0092-8674(01)00596-7 (2001).
33. Guo, X., Bernard, A., Orlando, D. A., Haase, S. B. & Hartemink, A. J. Branching process deconvolution algorithm reveals a detailed cell-cycle transcription program. *Proc. Natl. Acad. Sci. U. S. A.* **110**, E968-977. https://doi.org/10.1073/pnas.1120991110 (2013).
34. Kuranda, M. J. & Robbins, P. W. Chitinase is required for cell separation during growth of *Saccharomyces cerevisiae*. *J. Biol. Chem.* **266**, 19758–19767 (1991).
35. Baladrón, V. et al. Eng1p, an endo-1,3-beta-glucanase localized at the daughter side of the septum, is involved in cell separation in *Saccharomyces cerevisiae*. *Eukaryot. Cell.* **1**, 774–786. https://doi.org/10.1128/EC.1.5.774-786.2002 (2002).
36. Brace, J. L., Doerfler, M. D. & Weiss, E. L. A cell separation checkpoint that enforces the proper order of late cytokinetic events. *J. Cell Biol.* **218**, 150–170. https://doi.org/10.1083/jcb.201805100 (2019).

37. Foltman, M. et al. TOR complex 1 negatively regulates NDR kinase Cbk1 to control cell separation in budding yeast. *PLoS Biol.* **21**, e3002263. https://doi.org/10.1371/journal.pbio.3002263 (2023).
38. Mei, K. & Guo, W. The exocyst complex. *Curr. Biol.* **28**, R922–R925. https://doi.org/10.1016/j.cub.2018.06.042 (2018).
39. Mostowy, S. & Cossart, P. Septins: the fourth component of the cytoskeleton. *Nat. Rev. Mol. Cell. Biol.* **13**, 183–194. https://doi.org/10.1038/nrm3284 (2012).
40. Marquardt, J., Chen, X. & Bi, E. Septin assembly and remodeling at the cell division site during the cell cycle. *Front. Cell Dev. Biol.* **9**, 793920. https://doi.org/10.3389/fcell.2021.793920 (2021).
41. Okada, H., Ohnuki, S., Roncero, C., Konopka, J. B. & Ohya, Y. Distinct roles of cell wall biogenesis in yeast morphogenesis as revealed by multivariate analysis of high-dimensional morphometric data. *Mol. Biol. Cell.* **25**, 222–233. https://doi.org/10.1091/mbc.E13-07-0396 (2014).
42. Piotrowski, J. S. et al. Plant-derived antifungal agent poacic acid targets beta-1,3-glucan. *Proc. Natl. Acad. Sci. U.S.A.* **112**, E1490–1497. https://doi.org/10.1073/pnas.1410400112 (2015).
43. Spiridon-Bodi, M., Ros-Carrero, C., Igual, J. C. & Gomar-Alba, M. Dual regulation of the levels and function of Start transcriptional repressors drives G1 arrest in response to cell wall stress. *Cell. Commun. Signal.* **23**, 31. https://doi.org/10.1186/s12964-025-02027-z (2025).
44. Bermejo, C. et al. The sequential activation of the yeast HOG and SLT2 pathways is required for cell survival to cell wall stress. *Mol. Biol. Cell.* **19**, 1113–1124. https://doi.org/10.1091/mbc.e07-08-0742 (2008).
45. Shaw, J. A. et al. The function of chitin synthases 2 and 3 in the *Saccharomyces cerevisiae* cell cycle. *J. Cell Biol.* **114**, 111–123. https://doi.org/10.1083/jcb.114.1.111 (1991).
46. Smits, G. J., van den Ende, H. & Klis, F. M. Differential regulation of cell wall biogenesis during growth and development in yeast. *Microbiology* **147**, 781–794. https://doi.org/10.1099/00221287-147-4-781 (2001).
47. Back, S. H., Schroder, M., Lee, K., Zhang, K. & Kaufman, R. J. ER stress signaling by regulated splicing: IRE1/HAC1/XBP1. *Methods* **35**, 395–416. https://doi.org/10.1016/j.ymeth.2005.03.001 (2005).
48. Rodríguez-Peña, J. M., Díez-Muñiz, S., Bermejo, C., Nombela, C. & Arroyo, J. Activation of the yeast cell wall integrity MAPK pathway by zymolyase depends on protease and glucanase activities and requires the mucin-like protein Hkr1 but not Msb2. *FEBS Lett.* **587**, 3675–3680. https://doi.org/10.1016/j.febslet.2013.09.030 (2013).
49. González-Rubio, G., Martín, H. & Molina, M. The mitogen-activated protein kinase Slt2 promotes asymmetric cell cycle arrest and reduces TORC1-Sch9 signaling in yeast lacking the protein phosphatase Ptc1. *Microbiol. Spectr.* **11**e0524922. https://doi.org/10.1128/spectrum.05249-22 (2023).
50. Tamborrini, D. & Piatti, S. Septin clearance from the division site triggers cytokinesis in budding yeast. *Microb. Cell.* **6**, 295–298. https://doi.org/10.15698/mic2019.06.681 (2019).
51. McMurray, M. A. & Thorner, J. Reuse, replace, recycle. Specificity in subunit inheritance and assembly of higher-order septin structures during mitotic and meiotic division in budding yeast. *Cell. cycle.* **8**, 195–203. https://doi.org/10.4161/cc.8.2.7381 (2009).
52. DeMarini, D. J. et al. A septin-based hierarchy of proteins required for localized deposition of chitin in the *Saccharomyces cerevisiae* cell wall. *J. Cell. Biol.* **139**, 75–93. https://doi.org/10.1083/jcb.139.1.75 (1997).
53. Kozubowski, L. et al. A Bni4-Glc7 phosphatase complex that recruits chitin synthase to the site of bud emergence. *Mol. Biol. Cell.* **14**, 26–39. https://doi.org/10.1091/mbc.e02-06-0373 (2003).
54. Rodríguez-Peña, J. M., Rodríguez, C., Alvarez, A., Nombela, C. & Arroyo, J. Mechanisms for targeting of the *Saccharomyces cerevisiae* GPI-anchored cell wall protein Crh2p to polarised growth sites. *J. Cell. Sci.* **115**, 2549–2558. https://doi.org/10.1242/jcs.115.12.2549 (2002).
55. Oh, Y. & Bi, E. Septin structure and function in yeast and beyond. *Trends Cell Biol.* **21**, 141–148. https://doi.org/10.1016/j.tcb.2010.11.006 (2011).
56. van Drogen, F. & Peter, M. Spa2p functions as a scaffold-like protein to recruit the Mpk1p MAP kinase module to sites of polarized growth. *Curr. Biol.* **12**, 1698–1703. https://doi.org/10.1016/s0960-9822(02)01186-7 (2002).
57. González-Rubio, G., Sastre-Vergara, L., Molina, M., Martín, H. & Fernández-Acero, T. Substrates of the MAPK Slt2: Shaping yeast cell integrity. *J. Fungi* https://doi.org/10.3390/jof8040368 (2022).
58. García, R. et al. The global transcriptional response to transient cell wall damage in *Saccharomyces cerevisiae* and its regulation by the cell integrity signaling pathway. *J. Biol. Chem.* **279**, 15183–15195. https://doi.org/10.1074/jbc.M312954200 (2004).
59. O'Conallain, C., Doolin, M. T., Taggart, C., Thornton, F. & Butler, G. Regulated nuclear localisation of the yeast transcription factor Ace2p controls expression of chitinase (*CTS1*) in *Saccharomyces cerevisiae*. *Mol. Gen. Genet.* **262**, 275–282. https://doi.org/10.1007/s004380051084 (1999).
60. Okada, H., MacTaggart, B., Ohya, Y. & Bi, E. The kinetic landscape and interplay of protein networks in cytokinesis. *iScience* **24**, 101917. https://doi.org/10.1016/j.isci.2020.101917 (2021).
61. Yue, P. et al. Sec3 promotes the initial binary t-SNARE complex assembly and membrane fusion. *Nat. Commun.* **8**, 14236. https://doi.org/10.1038/ncomms14236 (2017).
62. Chao, J. T. et al. Transfer of the Septin Ring to Cytokinetic Remnants in ER Stress Directs Age-Sensitive Cell-Cycle Re-entry. *Dev. Cell* **51**, 173–191 e175. https://doi.org/10.1016/j.devcel.2019.08.017 (2019).
63. Singh, D. et al. Septins function in exocytosis via physical interactions with the exocyst complex in fission yeast cytokinesis. *eLife* **13** https://doi.org/10.7554/eLife.101113 (2025).
64. Wach, A., Brachat, A., Pohlmann, R. & Philippsen, P. New heterologous modules for classical or PCR-based gene disruptions in *Saccharomyces cerevisiae*. *Yeast* **10**, 1793–1808. https://doi.org/10.1002/yea.320101310 (1994).
65. Wach, A., Brachat, A., Alberti-Segui, C., Rebischung, C. & Philippsen, P. Heterologous *HIS3* marker and GFP reporter modules for PCR-targeting in *Saccharomyces cerevisiae*. *Yeast* **13**, 1065–1075. https://doi.org/10.1002/(SICI)1097-0061(19970915)13:11%3C1065::AID-YEA159%3E3.0.CO;2-K (1997).
66. Fang, X. et al. Biphasic targeting and cleavage furrow ingression directed by the tail of a myosin II. *J. Cell Biol.* **191**, 1333–1350. https://doi.org/10.1083/jcb.201005134 (2010).
67. Barberis, M. et al. Sic1 plays a role in timing and oscillatory behaviour of B-type cyclins. *Biotechnol. Adv.* **30**, 108–130. https://doi.org/10.1016/j.biotechadv.2011.09.004 (2012).
68. Manukyan, A., Abraham, L., Dungrawala, H. & Schneider, B. L. Synchronization of yeast. *Methods Mol. Biol.* **761**, 173–200. https://doi.org/10.1007/978-1-61779-182-6_12 (2011).
69. Juanes, M. A. Methods of Synchronization of Yeast Cells for the Analysis of Cell Cycle Progression. *Methods Mol. Biol.* **1505**, 19–34. https://doi.org/10.1007/978-1-4939-6502-1_2 (2017).
70. Blanco, N., Reidy, M., Arroyo, J. & Cabib, E. Cross-links in the cell wall of budding yeast control morphogenesis at the mother-bud neck. *J. Cell. Sci.* **125**, 5781–5789. https://doi.org/10.1242/jcs.110460 (2012).
71. García, R. et al. Genomic profiling of fungal cell wall-interfering compounds: Identification of a common gene signature. *BMC Genomics* **16**, 683. https://doi.org/10.1186/s12864-015-1879-4 (2015).
72. Livak, K. J. & Schmittgen, T. D. Analysis of relative gene expression data using real-time quantitative PCR and the 2(-Delta Delta C(T)) Method. *Methods* **25**, 402–408. https://doi.org/10.1006/meth.2001.1262

Acknowledgements

We thank the staff of CNME (Centro Nacional de Microscopía Electrónica) and the Genomics Unit (Jesús

García-Cantalejo, Pedro Botías, and Rosa Pérez) at the Universidad Complutense de Madrid (UCM) for their help with the electron microscopy and RT-qPCR experiments, respectively. We would like to express our sincere gratitude to Dr. Erfei Bi from the Department of Cell and Developmental Biology at the Perelman School of Medicine, University of Pennsylvania (Philadelphia, PA, USA), for kindly providing us with GFP-tagged yeast strains, to David E. Levin (Department of Molecular & Cell Biology at the Henry M. Goldman School of Dental Medicine, Boston University, MA, USA) for providing us plasmids p2188, p2190 and p2193, to Teresa Fernández-Acero (Departamento de Microbiología y Parasitología, Facultad de Farmacia, Universidad Complutense de Madrid, Spain) for providing us the plasmid YIn211-CDC3-mCherry and to Dr. Francesc Posas (IRB Barcelona - Institute for Research in Biomedicine, Barcelona, Spain) for providing us with the YAN48 strain. All members of our research group (UCM-920640: Yeast Functional Genomics) at the Department of Microbiology and Parasitology (UCM) are also acknowledged for their support. This work was supported by grants PID2019-105223GB-I00/AEI/10.13039/501100011033 and PID2022-136888NB-I00/AEI/10.13039/501100011033 to JA, and PID2020-118109RB-I00 to C.R.V.A., funded by Ministerio de Ciencia e Innovación/Agencia Estatal de Investigación, Spain. Y.P. was the recipient of the research contract (Laboratory technician) PEJ-2018-TL/BMD-11487 from Consejería de Educación e Investigación de la Comunidad de Madrid y del Fondo Social Europeo.

Author contributions

R.G. performed the experiments, collected and analyzed the data, interpreted the results, and reviewed the manuscript. J.M.R.-P. conceived and designed the study, analyzed the data, supervised the work, and wrote the first draft of the manuscript. S.D.-M. and Y.P. performed experiments. A.M.-L. performed confocal fluorescent microscopy experiments. C.R.V.A. performed confocal fluorescent microscopy experiments, designed experiments, interpreted results, and reviewed and edited the manuscript. J.A. conceived, designed, and supervised the study and reviewed the manuscript. All authors read and approved the final version of the manuscript.

Funding

Open Access funding provided thanks to the CRUE-CSIC agreement with Springer Nature.

Declarations

Competing interests

The authors declare no competing interests.

Additional information

Supplementary Information The online version contains supplementary material available at https://doi.org/10.1038/s41598-026-62018-z.

Correspondence and requests for materials should be addressed to C.R.V.d.A. or J.A.

Reprints and permissions information is available at www.nature.com/reprints.

Publisher's note Springer Nature remains neutral with regard to jurisdictional claims in published maps and institutional affiliations.

Open Access This article is licensed under a Creative Commons Attribution 4.0 International License, which permits use, sharing, adaptation, distribution and reproduction in any medium or format, as long as you give appropriate credit to the original author(s) and the source, provide a link to the Creative Commons licence, and indicate if changes were made. The images or other third party material in this article are included in the article's Creative Commons licence, unless indicated otherwise in a credit line to the material. If material is not included in the article's Creative Commons licence and your intended use is not permitted by statutory regulation or exceeds the permitted use, you will need to obtain permission directly from the copyright holder. To view a copy of this licence, visit http://creativecommons.org/licenses/by/4.0/.

© The Author(s) 2026